Spin and angle resolved photoemission on non-magnetic low-dimensional systems

2009 J. Phys.: Condens. Matter 21 403001

(http://iopscience.iop.org/0953-8984/21/40/403001)

IOP PUBLISHING JOURNAL OF PHYSICS: CONDENSED MATTER

J. Phys.: Condens. Matter **21** (2009) 403001 (22pp) doi:10.1088/0953-8984/21/40/403001

TOPICAL REVIEW

Spin and angle resolved photoemission on non-magnetic low-dimensional systems

J Hugo Dil

Physik-Institut, Universität Zürich, Winterthurerstrasse 190, 8057 Zürich, Switzerland
and
Swiss Light Source, Paul Scherrer Institute, 5232 Villigen PSI, Switzerland

E-mail: jan-hugo.dil@psi.ch

Received 10 July 2009, in final form 19 August 2009
Published 17 September 2009
Online at stacks.iop.org/JPhysCM/21/403001

Abstract

The electronic structure of non-magnetic low-dimensional materials can acquire a spin structure due to the breaking of the inversion symmetry at the surface or interface. This so-called Rashba effect is a prime candidate for the manipulation of the electron spin without using any magnetic fields. This is crucial for the emerging field of spintronics, where the spin of the electron instead of its charge is used to transport or store information. Spin and angle resolved photoemission is currently one of the main experimental methods to measure the spin resolved electronic structure, which contains all the relevant information for spintronics. In this review, the technique of spin and angle resolved photoemission will be explained and recent results on low-dimensional non-magnetic structures will be discussed.

(Some figures in this article are in colour only in the electronic version)

Contents

1. Introduction

The manipulation and measurement of the spin of an electron has received increasing attention in recent years. This is primarily driven by the prospect of a technology which is no longer based on the charge of the electron but rather on its spin, which is commonly referred to as spintronics [1]. In semiconductor technology, advancements in manipulating the spin–orbit interaction in two-dimensional electron gases are steady [2], although the determination of the spin of the electron primarily occurs by means of indirect measurements and modelling. Currently there is no reason to doubt the spin orientation which is determined by the combination of these experiments with state-of-the-art theory, but a more direct determination of the spin quantization axis would be desirable. Unfortunately this is not possible with the experimental techniques currently available, partly due to the relatively thick cover layers on top of the sample.

The observation of spin–orbit splitting in the Au(111) L-gap surface state by LaShell *et al* [3], was the first observation of a Rashba-type effect on the surface of a crystal and opened up the possibility to study such effects by photoemission. The next step was the use of spin and angle resolved photoemission to actually determine the spin orientation of the spin split bands. As will be described in more detail below, the spin polarization vector typically lies in the surface plane and changes sign for the spin split bands. However, for more complex systems the spin polarization vector can be rotated

out of the surface plane [4] and a manipulation of the spin polarization vector seems feasible [5].

In this non-comprehensive review the focus will lie on the spin structure of non-magnetic surfaces and low-dimensional systems. Crucial for the determination of the spin structure is of course the measurement of the spin expectation value, commonly referred to as spin polarization. In section 2 the currently available spin detection possibilities in light of spin and angle resolved photoemission will be shortly reviewed, including their (dis)advantages. The lifting of the spin degeneracy will primarily be caused by Rashba-type effects, the relevant physical background of which will be reviewed in section 3. With the increasing complexity of the systems under investigation, the necessity of a data analysis model which can extract subtle changes in the spin polarization vector has become apparent. In section 4 such an analysis routine and challenges in the data interpretation will be discussed. In section 5 some results obtained on clean and reconstructed surfaces, on systems involving thin metal films and on 'novel' materials such as graphene and topological metals will be highlighted.

2. Technical background of spin and angle resolved photoemission

Over the last couple of decades, angle resolved photoelectron spectroscopy (ARPES) has established itself as a powerful tool for the study of the electronic structure of surfaces or near surface regions [6]. One of the main advantages of ARPES is that one can simultaneously determine the binding energy and momentum of the electrons in the sample. The binding energy can be determined from the measured kinetic energy E_k, the used photon energy $\hbar\omega$ and the work function Φ as

$$E_b = \hbar\omega - E_k - \Phi. \tag{1}$$

The in-plane momentum of the electron in the solid $\mathbf{k}_\parallel$ can be determined from the measured kinetic energy and exit angle θ through

$$\mathbf{k}_\parallel = \sqrt{\frac{2m_e E_k}{\hbar^2}}\sin\theta. \tag{2}$$

These are two of the three main observables of an electron, the third one being the spin. The goal of spin and angle resolved photoelectron spectroscopy (SARPES) is to measure all these quantum numbers simultaneously. In order to achieve this, one could first filter the photoemitted electrons based on their kinetic energy and their exit angle and then feed this electron beam in a spin separator that would measure the up or down spin currents with respect to a given coordinate axis. Ideally one would thus use a Stern–Gerlach-type spin separator with a spatial detector, however such a spin separator does not work for charged particles such as electrons [7, 8].

Currently the most popular detection mechanisms are based on scattering asymmetries from crystalline solids and can be generalized in three different classes. Spin polarized low energy electron diffraction (SPLEED) relies on the different scattering probabilities of low energy (104.5 eV) electrons off a W(110) surface [9]. More specifically, on the differences in intensity between the $(2, 0)$ and $(\bar{2}, 0)$ diffraction spots to obtain the spin asymmetry in the direction perpendicular to the plane harbouring these rods. The main advantage of SPLEED is the relatively high sensitivity that can be obtained. A downside of this detection scheme is, however, that it strongly depends on the cleanliness of the W(110) crystal and on small changes in the electron energy. A further disadvantage is the strong dependence on incidence angle and that there is no intrinsic focusing due to the electron acceleration, which can be a source of instabilities and therefore reduces the detection accuracy.

In very low energy electron diffraction (VLEED) the spin-exchange interaction of a specular reflected electron beam of a magnetized thin film is used to obtain spin contrast [10]. Close to the edges of the unoccupied band gap of a ferromagnetic material the reflection probability of an electron strongly depends on its spin orientation with respect to the spin of the band closest to the absolute gap. The measurement has to be repeated with the target in the opposite magnetization state to obtain the spin asymmetry. In order to measure the two spatial directions, which are typically obtained simultaneously in a diffractive scattering detector, one therefore has to perform a total of four measurements. Luckily, the efficiency of such a detector is very high due to the low energy specular scattering, which in turn saves a lot of time. The downside of this low energy (10 eV) is that the scattering process strongly depends on the surface quality and could therefore rapidly change with time. However, it has been found that the target does not need to be metallic and an oxygen passivated iron film, Fe(001)–p(1 × 1)–O, can also be used with a kinetic energy of 6 eV [11]. This dramatically increases the lifetime of the target and enhances the stability of the instrument. Many promising developments based on this type of detector are currently underway [12, 13] and especially in combination with a time-of-flight (TOF) detector this might be a powerful type of spin detector [14]. Hopefully first results that will allow for an estimate of the accuracy and the stability of such instruments will soon be published.

Besides SPLEED and VLEED the third spin detection scheme is the Mott detector, which is currently the 'work horse' in spin resolved spectroscopy. This kind of detector is based on the spin dependent scattering of electrons from heavy nuclei at high ($\geqslant$25 kV) kinetic energies, first discussed by Mott in 1929 [7]. The principle of operation is that electrons scattered off, for example, a thin gold foil have a higher probability to be scattered to the left (right) when they have spin up (down) with regard to a given geometrical plane perpendicular to the surface of the foil [8]. The spin asymmetry A can be calculated as

$$A = \frac{N_L - N_R}{N_L + N_R}, \tag{3}$$

where N_L and N_R are the number of electrons counted in the detectors on the left- and right-hand side, respectively. From this asymmetry the spin polarization P of the photoelectrons can be determined as

$$P = \frac{A}{S}, \tag{4}$$

where S is the Sherman function [15] which determines the asymmetry that will be measured for a fully spin polarized electron beam. Together with the total measured intensity $I_t = N_L + N_R$ the obtained polarization yields the spin resolved intensity spectra

$$I_{up} = (1 + P)I_t/2 \qquad I_{dn} = (1 - P)I_t/2. \tag{5}$$

For magnetic systems with a well defined spin quantization axis, determined by the global magnetization direction of the sample, these spectra contain the full spin information because in principle the sample can always be aligned to let the magnetization and measurement direction coincide. However, as will be elucidated in section 3, non-magnetic systems can have spin structures where it is not possible to define a single quantization axis. This means that, in order to give sensible statements about the spin structure, more than one spatial direction should be measured. A second spatial direction, orthogonal to the first one, is obtained 'for free' from the scattering off the same gold foil. From a single Mott detector, the spin polarization along two spatial directions can thus be measured simultaneously. In a typical experimental set-up these two directions span the surface plane of the sample, but do not give any information about the out-of-plane spin polarization. In order to simultaneously measure the two in-plane directions and the out-of-plane direction a three-dimensional spin detector based on two orthogonal Mott detectors has been developed and built in our group [16, 17].

In this set-up the electrons are first energy and angle-filtered through a hemispherical electrostatic analyser after which the electrons are extracted from the analyser and accelerated through an electrostatic lens. This extractions lens is followed by a 90° bend and a ±45° electrostatic chopper operating at a frequency of 2 Hz, before the electrons are accelerated to 40 kV onto the Mott detector. This set-up is schematically shown in figure 1 and one can see that in total the electron trajectory has been first bent by 180° in the analyser, then back by 90° in the lens in one plane and bent by 45° in the perpendicular plane. Here it is of crucial importance that the spin of an electron is not affected by these electrostatic manipulations and, similar to the conservation of angular momentum, remains oriented along the same absolute direction in the laboratory coordinate frame. In this set-up the three-dimensional spin polarization is therefore measured in a coordinate frame which is rotated by 45° in the xy-plane with respect to the sample coordinate frame. Because in this set-up the polar angle θ of the sample is changed to access different emission angles, and the electron optics and Mott detectors stay fixed, the out-of-plane spin polarization in the sample coordinates will be partly projected on the in-plane direction of the Mott coordinates and vice versa. Therefore the spin polarization obtained in the Mott coordinate frame needs to be transferred to the sample coordinate frame by using a transformation matrix T which depends on the polar angle of the sample. For a single polar angle, this rotation matrix is defined as:

$$T = \frac{1}{\sqrt{2}} \begin{pmatrix} \cos\theta & -\cos\theta & \sqrt{2}\sin\theta \\ 1 & 1 & 0 \\ -\sin\theta & \sin\theta & \sqrt{2}\cos\theta \end{pmatrix}. \tag{6}$$

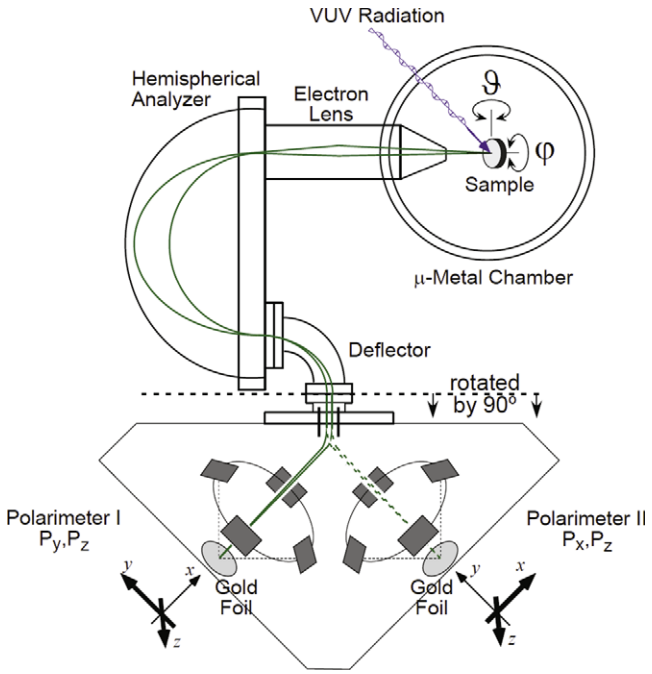

Figure 1. Experimental set-up of the complete photoemission experiment (COPHEE) at the surface and interface spectroscopy beamline at the Swiss Light Source. The photoemitted electrons first pass a hemispherical electrostatic analyser and are then accelerated through an electron lens with chopper, onto the Mott detectors. This configuration allows for the simultaneous detection of the binding energy, momentum and all three components of the spin polarization vector of the electron. Reproduced with permission from [16].

After this transformation a single measurement provides four data sets: the total intensity I_t and the spin polarization along the three spatial coordinates P_x, P_y, and P_z. From these the spin resolved spectra projected on the three spatial coordinates can be calculated according to equations (4) and (5), or, as will be shown in section 4, the full 3D spin polarization vector for each state can be determined.

In the preceding description of the Mott detector it has only been stated that the electrons are scattered off the thin gold foil at high kinetic energies and are successively detected at optimum scattering angles of 120°. However, to obtain a meaningful signal the inelastically scattered electrons have to be filtered out and removed from the main signal of elastically scattered electrons. Currently there are two primary detection schemes that successfully manage to do this, but both have their (dis)advantages. The first detection scheme is the conventional or classical Mott polarimeter [18] where the electrons are accelerated between two concentric hemispheres to 40–60 kV. The gold foil and the detectors (typically passivated implanted planar silicon (PIPS)) are at the same potential inside the inner hemisphere and the electrons thus travel through field free space between the foil and the detector [19]. The PIPS pulses are discriminated after amplification such that only the elastically scattered electrons are counted. A minimum of information is lost when the discriminators are set at a level where the dark count rate is slightly less than 1 Hz. The high potential difference between the exit of the Mott detector and the data acquisition electronics

is overcome by using fibre optics. The main advantage of this type of Mott detector is its high stability and reliability. The main disadvantage, that the polarimeter was very large because high voltages were used in order to be able to discriminate the background from the signal, has been resolved due to developments in detection technology [20]. The other main disadvantage is that the detectors, pre-amplifiers and discriminators are all at high voltage which results in rather complex electronics where standard components can not be easily integrated. Currently, several groups are very close to also solving this problem by using an all optical scheme after scattering.

The second type of Mott polarimeter is a retarding potential detector, which is often referred to as a Rice University type Mott detector [21]. Apart from some geometrical considerations, the main difference to the classical Mott polarimeter is that the electron detectors are at ground potential. Hence, after scattering off the gold foil the electrons enter a retarding field on their way to the channeltrons or plates. The background of slow inelastically scattered electrons is easily separated from the main signal in this field through the use of apertures. A further advantage is that all electronics are at ground potential and that the whole polarimeter can be made rather small and easily compatible with standard photoemission equipment. Furthermore, the efficiency of this type of Mott polarimeter is a bit higher as that of the classical Mott polarimeter, meaning that measurements take less time. The main downside of the retarding potential Mott is the relatively low stability. In a comparative study between a classical and a retarding potential type Mott polarimeter [22], Petrov and co-workers have found that whereas the conventional polarimeter shows no significant change in count rate when the incoming electron beam is shifted by a millimetre, the Rice Mott showed asymmetric intensity changes on the different detection channels of more than 10% for much smaller shifts. They attribute this difference in behaviour to a combination of two effects. First, the spherical geometry of the classical Mott focusses the electrons very well on the gold foil. Second, the electron trajectories after scattering of the gold foil may be changed drastically due to the retarding field. In a laboratory environment there are many factors that can influence the position of the electron beam on different timescales, which will result in high intensity fluctuations and thus a loss of accuracy for the retarding potential type Mott detector.

All the spin detectors listed above have their advantages and disadvantages, and the ideal polarimeter unfortunately does not exist yet. When considering the implementation of a spin detector in an experimental set-up, one has to decide which properties are most important for the experiments that one wants to perform with it and what other experimental parameters are available. For us the stability and reliability of the spin detector are of crucial importance because we want to be able to perform a quantitative analysis of the measured spin polarization. Therefore we decided to work with a compact classical Mott detector operated at 40 kV with PIPS detectors.

3. Basic theory of the Rashba effect

It is well known that in many cases the surface of a metal crystal is not just a truncation of the bulk [23]. A prime example of this is the different surface reconstructions of gold [24–26], which form because the packing of the atoms at the surface is denser than in the bulk. Furthermore, due to the confinement between a projected band gap and the image potential, surface states can form [27], which have totally different properties to the bulk electronic states. In both cases the main cause of the differences at the surface is that the translational symmetry is broken along the surface normal, or more specifically that the space inversion symmetry is broken.

For an electron with a given momentum $\vec{\mathbf{k}}$ and spin ($\uparrow$ or $\downarrow$), space inversion symmetry is represented by the idea that it is equivalent whether the electron moves in one direction or the other; i.e. $E(\vec{\mathbf{k}}, \uparrow) = E(-\vec{\mathbf{k}}, \uparrow)$. In the absence of open d-shells or magnetic fields, time inversion symmetry should also hold; i.e. $E(\vec{\mathbf{k}}, \uparrow) = E(-\vec{\mathbf{k}}, \downarrow)$. In the bulk of a non-magnetic metal both time and space inversion symmetry are observed, resulting the formation of spin degenerate states $E(\vec{\mathbf{k}}, \uparrow) = E(\vec{\mathbf{k}}, \downarrow)$. As indicated above, for states located at the surface the space inversion symmetry is broken, which means that the spin degeneracy does not necessarily hold for these states.

That the spin degeneracy is actually lifted for surface states can be understood by the following simple relativistic approach. The sudden termination of the crystal at the surface creates a potential gradient perpendicular to the surface, which can also be regarded as a local electric field. Through a Lorentz transformation this electric field becomes a magnetic field in the rest frame of a moving valence electron at the surface. This magnetic field causes a Zeeman splitting of the electronic states and thus an energy difference between the states with spin up and spin down. The magnitude of the magnetic field and thus also the energy splitting depends on the momentum of the electron and changes sign for opposite momenta. At zero momentum the splitting disappears and the bands become degenerate again.

This relativistic process can more formally be described along the lines of the Rashba–Bychkov effect [28, 29] (henceforth: Rashba or RB effect) by the following Hamiltonian [30, 31]:

$$H = H_0 + H_{\mathrm{RB}}, \tag{7}$$

where the energy of the two-dimensional electron gas with effective mass m^* and band offset $E_{\bar{\Gamma}}$ is

$$H_0 = \sigma_0 \left(E_{\bar{\Gamma}} - \frac{\hbar^2}{2m^*} \nabla^2 \right), \tag{8}$$

while the Rashba term is

$$H_{\mathrm{RB}} = -\alpha_{\mathrm{RB}} \left(\mathrm{i}\sigma_y \frac{\partial}{\partial x} - \mathrm{i}\sigma_x \frac{\partial}{\partial y} \right). \tag{9}$$

The coupling constant α_{RB} reflects the RB coupling. This Rashba constant is typically viewed as being composed of an atomic Z dependent contribution and a structural contribution

representing the potential gradient [30]. For positive α_{RB} the potential gradient is in the positive z-direction and for negative α_{RB} it is in the opposite direction [32]. The unit 2×2 matrix is denoted by σ_0, while σ_x and σ_y are the standard Pauli matrices in the basis in which the quantization axis is along the z direction. The eigenenergies of H yield the upper $(+)$ and lower $(-)$ Rashba branches

$$E_{\pm}(\boldsymbol{k}) = E_{\bar{\Gamma}} + \frac{\hbar^2|\boldsymbol{k}|^2}{2m^*} \pm \alpha_{RB}|\boldsymbol{k}|. \tag{10}$$

The eigenspinors corresponding to this Hamiltonian are

$$|\boldsymbol{k}, \pm\rangle = \frac{1}{\sqrt{2}}\left(e^{-i(\varphi \pm \pi/2)}, \quad 1\right), \tag{11}$$

where $\varphi = \arctan(k_y/k_x)$ and the two-dimensional momentum $\boldsymbol{k}$ is measured relative to the $\bar{\Gamma}$ point. In order to relate to measurements, it is better to consider the expectation value of the spinors:

$$\boldsymbol{S}_{\pm}(\boldsymbol{k}) = \frac{\hbar}{2}\begin{pmatrix} \mp \sin\varphi \\ \pm \cos\varphi \\ 0 \end{pmatrix}. \tag{12}$$

From this equation it is straightforward to determine the spin direction for different points in k-space. For the simple model described here the spin expectation vector is always perpendicular to the k-vector and has no out-of-plane component. The combination of equations (10) and (12) results in the picture for an ideal two-dimensional Rashba system as displayed in figure 2. A constant energy surface above the crossing point of the two parabolae consists of two concentric circles, where, for $\alpha_{RB} > 0$, the spin of the inner circle rotates clockwise and the spin of the outer circle counter-clockwise when regarded from the top. Instead of viewing the band splitting as an energy separation, one can also regard it as two bands that are shifted in momentum. One branch is shifted by k_0 to the left and the other by the same amount to the right, resulting in a total momentum splitting, at a given energy, of $2k_0$. This momentum splitting provides the phase difference in the spin field effect transistor proposed by Datta and Das and causes the necessary spin precession [33]. A larger momentum splitting will result in a faster spin rotation and can thus make such a device smaller.

As has been stated above, time reversal symmetry still holds for systems with a Rashba-type spin splitting, which can be verified by the observation that the spin polarization vector for k-vectors with different sign is opposite. A further consequence is that the bands have to cross at $\bar{\Gamma}$ because this is a centre of inversion symmetry, which is commonly referred to as a time reversal invariant momentum (TRIM). Based on similar symmetry considerations it is possible to identify other points in the surface Brillouin zone (SBZ) which are also protected by time inversion symmetry. These are the points which are located exactly between two $\bar{\Gamma}$ points of adjacent SBZs. For a surface with a hexagonal lattice structure this means that the $\bar{M}$ point is a TRIM and the Rashba split bands should cross here, whereas the $\bar{K}$ point is not protected by time reversal and more complex band and spin structures can be expected. A nice example of this increasing complexity for the spin structure, is the sudden out-of-plane rotation of the spin vector at the $\bar{K}$ point for Tl/Si(111) [34].

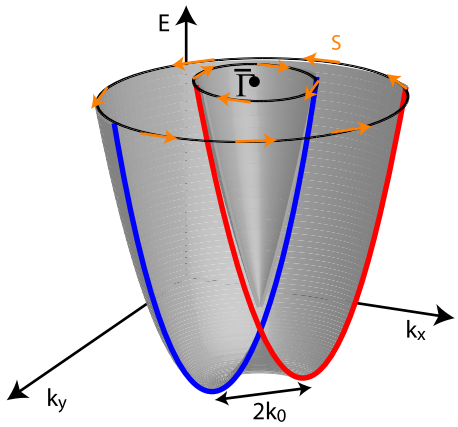

Figure 2. Band structure of a nearly free two-dimensional electron gas due to the Rashba effect. The two parabolae are each shifted by k_0 away from $\bar{\Gamma}$ resulting in a momentum dependent energy splitting.

The Rashba theory has been developed for two-dimensional electron gases in semiconductor heterostructures, this makes it remarkable that the first observation of a band splitting that could unambiguously be attributed to a Rashba-type effect was on a surface. In 1996 Jensen *et al* observed a splitting of the Au(111) surface state by angle resolved photoemission [3], one year before the observation by Nitta *et al* on an inverted $In_{0.53}Ga_{0.47}As/In_{0.52}Al_{0.48}As$ heterostructure [35]. Because it was the first of its kind and the result was rather unexpected, the paper by LaShell extensively discusses why the herringbone reconstruction of Au(111) [36] cannot be the cause of the observed splitting. Based on the further observations in similar systems, as will be discussed below, this interpretation certainly holds, but it remains difficult to estimate how much the surface corrugation due to this reconstruction actually enhances the Rashba-type spin splitting.

Triggered by the results for Au(111) a spin–orbit coupling induced band splitting was next observed and interpreted as such for the Li induced surface state on W(110) [37]. The first experimental verification of the spin structure by spin and angle resolved photoemission spectroscopy was performed on the related system of W(110)-(1×1)H [38]. In this work no out-of-plane spin polarization could be observed above the detection limit, which is in good correspondence to the predictions of the nearly free electron model described above and summarized by equation (12). That the spin polarization vectors are perpendicular to the k-vector of the electron throughout the SBZ is nicely illustrated in the first spin resolved Fermi surface map for a Rashba system obtained by Hoesch *et al* [39]. Also in this experiment no significant out-of-plane spin polarization could be detected, which further illustrates that the Rashba model is adequate for free electron like surface states.

Opposite to what one would expect, a large band splitting does not necessarily facilitate the data interpretation in terms of a Rashba-type effect. This is nicely illustrated by the many photoemission studies performed for the surface of Bi(111),

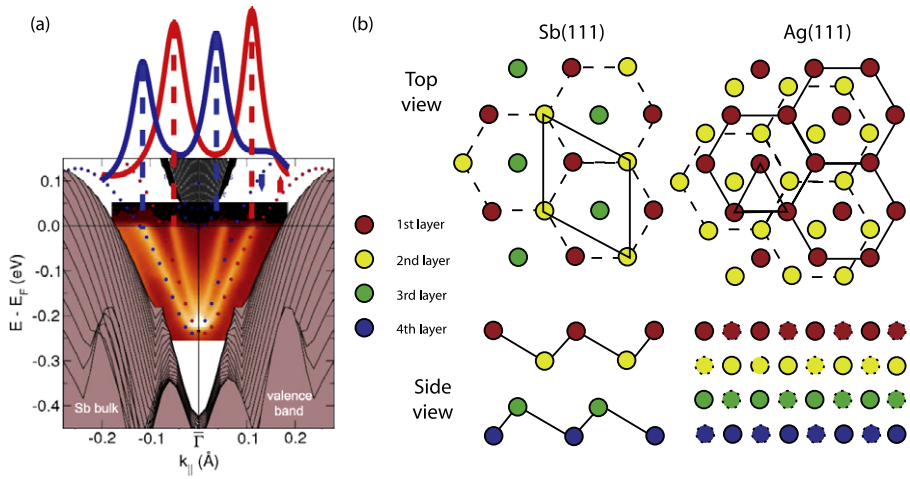

Figure 3. (a) Spin integrated ARPES band map of Sb(111) along the $\bar{\Gamma}\bar{M}$ direction, and spin resolved MDC of Sb(111) at the Fermi energy projected perpendicular to the measurement direction. The shaded area and dotted lines are obtained from DFT calculations and represent the Sb(111) bulk and surface states, respectively. Adapted from [50]. (b) Truncated crystal structure of rhombohedral Sb(111) and cubic Ag(111). The different colours indicate different layers and the different borders for Ag(111) indicate different locations in the perpendicular direction within this layer. The atom distances of Sb and Ag are not to scale.

as has been reviewed by Hofmann in 2006 [40]. Due to the very large splitting, the two Rashba branches of the Bi(111) surface state have long been interpreted as unrelated to each other even in high resolution ARPES measurements [41, 42]. This has for example resulted in the assumption of a charge density wave (CDW) on the Bi(111) surface [43] and a far too large number of electrons at the surface compared to the bulk. Fully relativistic band structure calculations in combination with further high resolution ARPES measurements on the Bi(100) and Bi(110) surfaces finally led to the conclusion that the surface states of bismuth show a strong Rashba-type spin splitting [44–46]. That the surface state bands are spin polarized and obey the time reversal symmetry demanded by the Rashba effect has been confirmed by SARPES measurements, although unfortunately the out-of-plane component of the spin polarization vector has not been determined [47].

Based on the increased spin–orbit splitting of the Bi surface state compared to the Au surface state one could easily assume that the band splitting directly depends on the atomic number. Under the assumption that all other factors are the same this is correct. However, as will be illustrated by Sb(111), for many cases the atomic structure can have a large influence. Antimony ($Z = 51$) is located in the row above bismuth ($Z = 83$) and gold ($Z = 79$) and is closer to silver ($Z = 47$). For the Ag(111) L-gap surface state no spin splitting can be observed, and from theoretical considerations it is expected that the total momentum splitting due to spin–orbit coupling is around 0.0013 Å^{-1} [48]. Based on the atomic weight, one would therefore expect that for Sb(111) a spin splitting of the surface state would also be below the detection limit. However, ARPES measurements performed by Sugawara *et al* provided first strong indications that spin–orbit coupling plays an important role for the Sb(111) surface state [49]. The Fermi surface is very similar to the Fermi surface of Bi(111) and the authors directly identified the electron and hole pockets as spin split pairs. Figure 3(a) shows more recent ARPES measurements with higher resolution which could identify the momentum splitting of the bottom of the two bands [50]. Due to the non-parabolic dispersion this yields the best comparison to the noble metal surface states. This splitting was found to be 0.03 Å^{-1} which is larger than for Au(111) (0.024 Å^{-1}) and more than 20 times larger than for Ag(111), which corresponds well to DFT calculations. The spin resolved ARPES measurements shown in the same figure have confirmed that the bands are spin split and that the spin polarization vectors follow the Rashba model described above, although there is also a slight out-of-plane component [50].

Antimony crystallizes in a rhombohedral structure typical for the group V semimetals. Like the other noble metals silver has a face centred cubic structure. In figure 3(c) the truncated bulk lattice structure for Sb(111) and Ag(111) are compared both for a top view and side view. The top view for both surfaces shows a very similar hexagonal structure and only the side view reveals the dramatic difference between the two crystal structures. Antimony clearly shows a bilayer type structure with alternating interlayer spacings and asymmetric atom positions with regard to the lower layers [51]. Ignoring the surface layer relaxation, the silver layer spacing is constant and the atoms have symmetric positions with regard to the deeper layers. The lattice structure of Sb results in a situation where the wavefunction distribution of the surface state is rather asymmetric around the atoms. This enhanced asymmetry can have a profound influence on the spin–orbit coupling according to the model proposed by Bihlmayer and co-workers to explain the microscopic origin of the Rashba effect [52]. This provides a clear indication that besides the atomic weight the exact crystal structure plays a decisive role in determining the size of the Rashba-type spin splitting. That a large surface corrugation can strongly enhance the spin splitting of surface states will be further illustrated by the surface alloys in section 5.1.

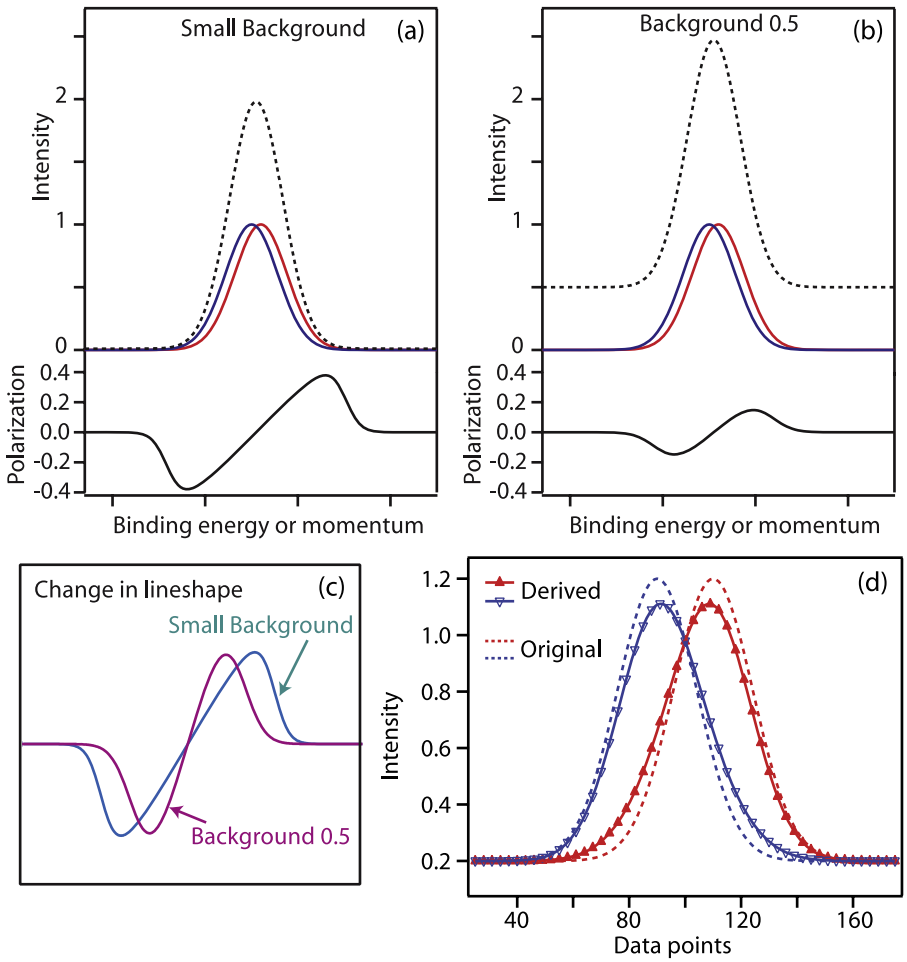

Figure 4. Challenges in the analysis of SARPES data without an adequate analysis routine. Polarization spectra for two overlapping peaks with (a) a very small and (b) a realistic background. (c) Normalized polarization spectra from (a) and (b) to indicate the change in line shape. (d) Original data (dashed lines) and spin resolved spectra projected on an axis that is rotated with 45° compared to the spin quantization axis (symbols and solid lines).

As has been indicated above, the Rashba effect for Ag(111) is very small, for Cu or lighter materials the momentum splitting will be even smaller and one can imagine that it eventually will approach zero. For these very small splittings, which are beyond any detection limit one can currently envisage, the bands are typically regarded as being degenerate. However, in some cases it can be important to realize that even if the band splitting approaches zero, the spin is still aligned along a quantization axis tangential to the constant energy contours. The spin up and down bands now almost fully overlap and for every energy and momentum there is an equal probability of finding the electron in a spin up or a spin down state along this quantization axis. This is different from the band degeneracy in the bulk of a centro-symmetric crystal where all spin directions are equally probable and there is no preferred spin quantization axis. To distinguish between these types of degeneracy sometimes the terms double and multiple degeneracy are used.

4. Importance of data analysis routine

In section 2 it has been explained that a typical SARPES data set consists of a total intensity spectrum I_t and polarization spectra along one or more spatial direction, P_α with $\alpha = x, y, z$. From this data set typically the spin resolved spectra projected on these spatial directions are calculated along the lines of equation (5). Conclusions about the electronic spin structure of the sample, such as band splitting and degree of polarization are then drawn from these or from the polarization spectra. Although such an analysis is certainly helpful to obtain a first overview, it can in many cases lead to precipitous conclusions. In this section some examples of this will be given and it will be shown how such mistakes can in principle be avoided.

For most non-magnetic systems the photoemission background is unpolarized and defines the zero level in the polarization spectra. However, this background can have a profound influence on both the shape and amplitude of the measured polarization spectra. In figures 4(a) and (b) the polarization spectra for two different peak to background ratios are displayed. Although the splitting and the intensities of the spin up and spin down bands are the same, the magnitude of the polarization is clearly reduced in the case of a higher background. This can be easily understood from the fact that, when the asymmetry is calculated according to equation (3), the influence of the background cancels in the numerator

whereas the denominator increases due to the background. Less intuitive is the change in polarization line shape for two overlapping bands with changing background as exemplified in figure 4(c), where the amplitude is normalized. The polarization maxima shift towards each other with increasing background and do not correspond to the position of the band maxima.

In a typical photoemission experiment there are many factors that can influence the background, such as sample and photon beam quality, secondary, inelastically and quasi-elastically scattered electrons, and the presence of unpolarized (bulk) bands. For a single sample, the background can depend on the kinetic energy and emission angle used in the measurement, and the background is, especially for energy distribution curves, not necessarily constant. Furthermore, the measured spin polarization directly depends on the amount of overlap between spin polarized bands, and thus also on the measurement resolution, the intrinsic linewidth, the sample temperature, the band splitting in degrees, and therefore the kinetic energy. Given this large number of influences on the polarization spectra it is rather perilous to draw any conclusions, beyond the existence of a spin splitting, from these spectra alone. In one of the earliest SARPES experiments on non-magnetic systems by Hochstrasser *et al* [38] the case is actually the opposite; the conclusions that are drawn about fully in-plane polarized bands seem to be correct but the polarization spectra that are shown are rather unexpected. They show a polarization amplitude close to 100%, which would only occur for fully polarized free-standing features without any background. This is obviously not the case in this experiment and one can assume that the authors have underestimated the magnitude of the Sherman function. On the other hand, Hochstrasser *et al* show a decrease of the measured polarization when the W(110) surface states cross into the bulk continuum, which they attribute to a loss of surface character. However, it should be noted that in this bulk continuum the peak to background ratio will decrease and subsequently also the measured spin polarization. Only a more detailed analysis where the background influence can be discriminated from any real decrease in intrinsic band polarization would be able to determine whether this intrinsic polarization really decreases. The two step fitting routine, which will be explained later in this section, can disentangle these different factors.

Figure 4(d) illustrates the result of choosing an axis other than the spin quantization axis to project the spin resolved spectra on. The original data sets consists of two fully polarized Gaussian lines with a spacing of 20 points. The polarization spectrum derived from these peaks is then divided by $\sqrt{2}$ to mimic a difference between the real and the assumed spin quantization axis of 45°. The spin resolved spectra calculated from this 'new' polarization spectrum still show two clear peaks with opposite spin orientation, but now the splitting is only 16 points, a reduction of 20%. If the discrepancy between the real spin quantization axis and the axis used for projection increases, the measured polarization along this axis strongly decreases, and the band splitting might seem to disappear. Especially in Rashba systems with very narrow Fermi surfaces, such as bismuth, where the spin quantization axis rapidly changes as a function of momentum, this may cause severe difficulties in the data interpretation based on polarization and spin resolved spectra alone [53]. Such difficulties can be circumvented by using the following analysis method.

In order to be able to perform a quantitative vectorial analysis of spin resolved ARPES data, a two step fitting routine has been developed in our group [4]. As a first step the total (spin integrated) intensity is analysed by fitting it with a background $B(E, \vec{\mathbf{k}})$ and the adequate number n and type of line shapes $I^i(E, \vec{\mathbf{k}})$; Gaussian, Lorentzian or more complex. This is a well established technique in the ARPES community and will not be discussed here any further. This first step separates, for each data point, the contributions from the individual bands and the background to the overall photoemission intensity. The result of this fit can be written as

$$I_t(E, \vec{\mathbf{k}}) = \sum_{i=1}^{n} I^i(E, \vec{\mathbf{k}}) + B(E, \vec{\mathbf{k}}). \tag{13}$$

In the second step of the fitting routine, a polarization vector $\vec{P}^i$ defined by two polar angles θ and ϕ and a length c is assigned to each peak as

$$\vec{P}^i = (P^i_x, P^i_y, P^i_z) = c_i(\cos\theta_i \cos\phi_i, \cos\theta_i \sin\phi_i, \sin\theta_i). \tag{14}$$

Combined with equation (13) the spin up and spin down intensities can now be calculated along each spatial axis and from this the polarization along this axis can be calculated from the inverse of equation (5). This *calculated* polarization is then fitted to the *measured* polarization by first varying the angles of the polarization vector and, if necessary, also the length. Here the background is assumed to be unpolarized, but could of course also be assigned its own polarization vector. Given the large number of total parameters that are used in both steps, certain physical constraints have to be taken into account during the fitting. In general several iterations have to be performed whereby also the spin integrated curve fitting has to be optimized. In many instances more than one fit of the total intensity is possible, especially if the different states strongly overlap. However, the simultaneous fitting of the spin polarization data will typically yield an unique total fit and set of spin polarization vectors. A more detailed description of this fitting routine can also be found in a recent tutorial by our group [54].

In this analysis method the spin polarization vector is always determined using the measured total intensity and background. This makes the routine robust against changes in the band intensity due to matrix element effects, whereas the individual polarization spectra can change dramatically in this case [54]. Conclusions based solely on the measured polarization spectra when changing the photon energy, emission angle or even binding energy, may, under the influence of strong matrix element effects, not hold. Here it should be noted that especially for systems involving heavy nuclei, where the spin orbit coupling is large, photoemission matrix element effects can also be substantial.

Unfortunately, not every experimental set-up has access to all three spatial components of the spin polarization. However,

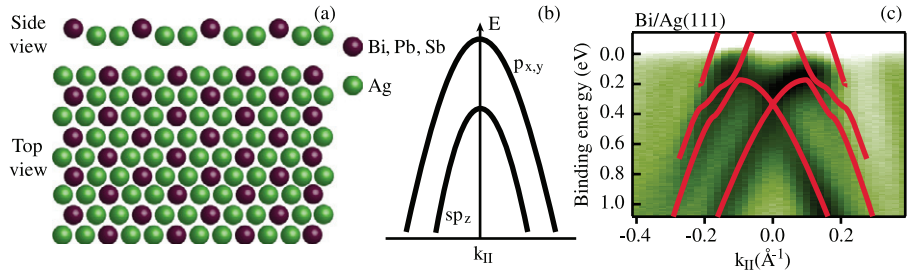

Figure 5. General atomic structure (a) and electronic structure without spin orbit coupling (b) of the Bi, Pb, or Sb surface alloys on Ag(111). (c) Measured spin integrated band structure for Bi/Ag(111) at $h\nu = 24$ eV along the $\bar{\Gamma}\bar{M}$ direction from [4]. The solid lines represent the calculated band structure from [56].

this does not mean that the analysis routine described above can not be applied. From the theoretical background of the Rashba effect described in section 3 it follows that in principle fully polarized individual states can be expected. This has been verified by many of the results in the following sections where a full three-dimensional vectorial analysis has been performed. Under this assumption, the two orthogonal measurement directions that are obtained from a diffraction type spin polarimeter suffice to perform a complete vectorial analysis. As a result of this analysis one will even obtain the missing polarization spectrum, where the sign of the polarization of the individual bands should be determined from further considerations. For measurements with a uni-axial spin polarization and fully polarized bands, the fitting of a single measurement direction is of course also helpful to discriminate the influence of the background, but many fine details and unexpected results may be missed in this case.

To conclude, a first idea about the spin resolved band structure of a sample can be obtained by a quick analysis of the measured polarization curves and the spin resolved intensities that are derived from them. In order to be able to make any quantitative statements about the spin structure, a more detailed analysis is necessary that eliminates the influence of the unpolarized background and the overlapping of different bands. The vectorial two step fitting method described here, can separate these influences and yields the spin polarization vector for each individual state.

5. SARPES results for novel low-dimensional structures

In section 3 (S)ARPES results for Rashba-type spin splitting of surface states on low index single crystals have been discussed. In the following sections recent results of non-magnetic spin effects on a variety of low-dimensional structures will be reviewed. In the first part long range ordered surface alloys are discussed which serve as ideal model systems because of the large band splitting. The second part deals with spin effects in thin metal films, either through hybridization effects or intrinsic Rashba-type effects. The last part discusses possible spin splittings in graphene, and exciting new results on topological metals and insulators.

5.1. Enhanced Rashba effect in surface alloys

The long range ordered $(\sqrt{3} \times \sqrt{3})$R30° surface alloys of Pb, Bi and Sb on Ag(111) are a family of materials with relatively strong spin orbit coupling effects in the valence band structure. Figure 5(a) schematically shows the general atomic structure of these surface alloys which are formed for 1/3 of a monolayer of Bi, Pb or Sb on Ag(111). The unit cell consists of three atoms, where every third Ag atom is substituted by a foreign atom which makes the structure decidedly different from an adsorbate induced surface reconstruction such as for example the different $(\sqrt{3} \times \sqrt{3})$R30° phases of Pb on Si(111) [55]. In the side view only the top atomic layer is displayed for the sake of simplicity and the incorporation of the adatoms in the surface structure is clear. This means that although the surface is ordered, it is best described as an alloy. The Bi/Pb/Sb atoms are not in the same plane as the topmost Ag atoms. As will be discussed below, this surface corrugation plays an important role for the magnitude of the Rashba-type effects in these systems.

The general electronic structure of these surface alloys consists of hole like surface states with a low effective mass, as displayed in figure 5(b). The lower or inner state has primarily sp_z character and the outer bands have mostly $p_{x,y}$ symmetry. The band filling is determined by the number of valence electrons of the substituent. In a first approximation the inner bands are rotational symmetric around $\bar{\Gamma}$ whereas the dispersion of the outer bands shows a dependency on crystal orientation. In contrast to the noble metal surface states, the surface states of the surface alloys are strongly localized in the top layer and hardly penetrate into the crystal. This makes them very sensitive even to small changes in the atomic surface structure.

The surface structure of the long range ordered surface alloy of Pb/Ag(111)$(\sqrt{3} \times \sqrt{3})$R30° has been studied by LEED and Auger spectroscopy [57, 58] and after some debate the structure has eventually been solved by surface x-ray diffraction (SXRD) [59]. In this SXRD study it was found that the Pb atoms are located approximately 0.47 Å above the plane of the Ag atoms. This large surface corrugation has a profound influence on the electronic structure of the Pb induced surface states. Spin integrated ARPES measurements revealed that the degeneracy of the inner surface states is lifted and that they are actually split by $2k_0 = 0.06$ Å^{-1} [60]. This splitting is more

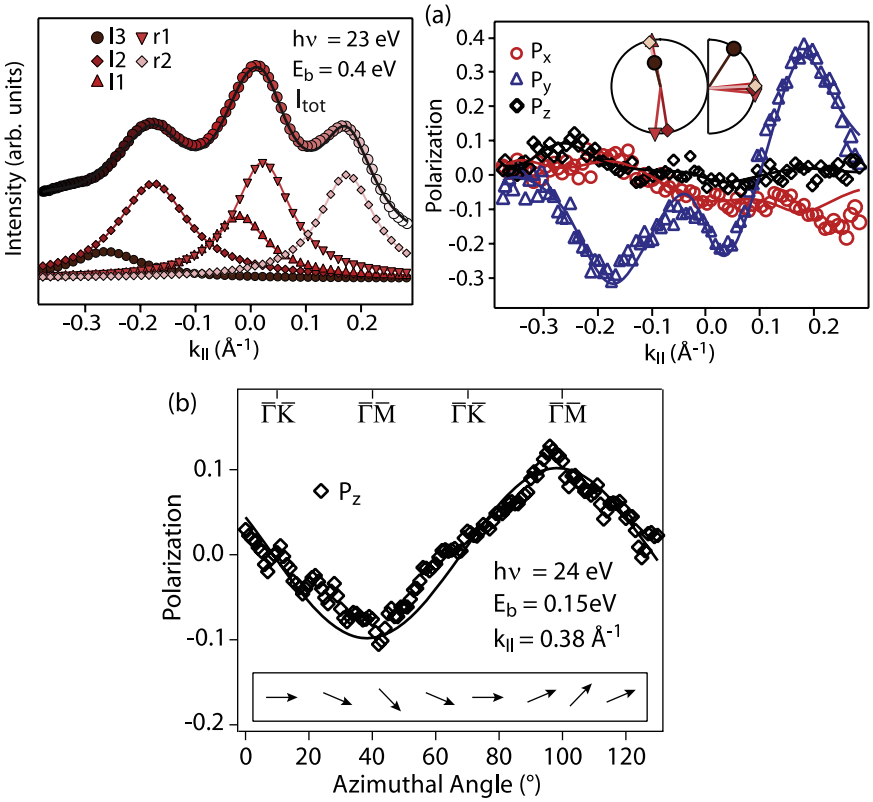

Figure 6. (a) Spin resolved MDC for Bi/Ag(111) at a binding energy of 0.4 eV and a photon energy of 23 eV. The left panel shows the spin integrated data with the peaks used for fitting. The right panel shows the measured and fitted polarization spectra based on the spin polarization vectors in the inset. (b) Out-of-plane spin polarization as a function of azimuthal angle for Pb/Ag(111). Based on further data it can be determined that the spin polarization vector oscillates as shown in the inset. Reproduced with permission from [4]. Copyright 2008 by the American Physical Society.

than twice as large as for the Au(111) surface state [3] and comparable to the splittings observed on bismuth surfaces [45].

A further breakthrough in Rashba-type spin–orbit coupling effects on surfaces was reached with the study of the Bi/Ag(111)($\sqrt{3} \times \sqrt{3}$)R30° surface alloy. Because of the additional valence electron of Bi compared to Pb, the bands are more filled and the inner surface state is fully occupied. ARPES measurements on this system show that the band splitting of the inner surface states is $2k_0 = 0.26$ Å^{-1} [61]. This band structure is also displayed in figure 5(c). Using the support of fully relativistic band structure calculations, Ast and co-workers could show that the bands are spin polarized and that the spin polarization vector should posses a considerable out-of-plane component that varies with crystal orientation.

These unexpectedly large Rashba-type effects triggered the search for a theoretical explanation of the spin splitting in surface alloys. In the first approach Premper *et al* explain the effect using a nearly free electron model with both an out-of-plane and in-plane potential gradient [62]. The idea is that the difference between the Ag and Bi (or Pb) atoms creates an additional potential gradient in the surface plane. The superposition of these orthogonal potential gradients results in a spin splitting which is much larger than just the sum of both effects. The second approach by Bihlmayer *et al* was to perform first principle fully relativistic density functional theory calculations with and without spin–orbit coupling and as a function of surface corrugation [56]. As expected, the band splitting disappears if the spin–orbit coupling is switched off, which confirms the relativistic nature of the effect. More intriguing is that the spin splitting and the binding energy of the crossing point directly depend on the outward relaxation of the Pb or Bi atoms; if the corrugation is smaller, the band splitting is also smaller. This means that apart from a small influence of the difference in spin orbit coupling parameter, the difference between the spin splitting of the Pb/Ag(111) and Bi/Ag(111) surface alloys can probably be explained by the difference in outward relaxation, where the surface corrugation is larger for Bi/Ag(111). Ongoing structural determinations of both surface alloys seem to support this hypothesis.

The proposed spin structure of the surface alloy surface states, consisting of tangential spin polarization vectors in accord with the Rashba model, has been confirmed by spin resolved ARPES [4]. Using the two step fitting routine described in section 4 it could be verified that the bands are fully polarized. Further, the spin polarization vector could be determined also for strongly overlapping bands where the polarization spectra and spin resolved spectra are hard to interpret. This is exemplified by the momentum distribution curve (MDC) shown in figure 6(a) obtained for a measurement almost exactly through the crossing point of the surface state bands of Bi/Ag(111); $E_b = 0.4$ eV. In the spin integrated data only three peaks can be discerned and the y-polarization spectrum shows a variety of oscillations. The data analysis, however, clearly indicates that the main features are formed

by four bands with alternating spin orientation and that the asymmetry around normal emission is induced by different intensities of the spin up and down features. The inset in the right panel of figure 6(a) shows the x and y component of the spin polarization vector on the circle and the out-of-plane component on the half-circle. The symbols represent which band the polarization vector applies to, and correspond to the symbols of the bands in the left panel.

At around $k_{\parallel} = -0.25$ Å^{-1} a small peak in the out-of-plane (z) polarization can be observed which disperses with binding energy; for $E_b = 0.9$ eV, $k_{\parallel} = -0.35$ Å^{-1} [4]. A more detailed analysis indicated that this z-polarization is caused by a $p_{x,y}$ derived band. This out-of-plane polarization component, which has also been predicted by theory [61, 62], can in a first approach be understood based on simple geometrical arguments. The $p_{x,y}$ bands are more sensitive to the in-plane asymmetry or potential gradient and just like a potential gradient along the z-direction will cause a y-polarization for states propagating along the x-direction, a potential gradient along the y-direction will cause an out-of-plane polarization component. For a more detailed description one has to consider the mixing of the wavefunctions and their spatial distribution [56], but this goes beyond the scope of this review.

For Pb/Ag(111) the spin structure is very similar to that of Bi/Ag(111), just with a smaller Rashba splitting. Also the out-of-plane component of the polarization of the $p_{x,y}$ bands has the comparable value of around 50° [4]. In order to obey time inversion symmetry for this spin component a six-fold spin symmetry is not possible, and a three-fold symmetry is expected. That the out-of-plane spin polarization is coupled to the crystal lattice can be verified by the dependence on azimuthal angle or crystal orientation. In figure 6(b) the measured z-polarization is displayed as a function of crystal orientation[1]. In this measurement the polar detection angle and kinetic energy are kept constant while rotating the azimuthal angle. Although the same state is continuously probed, the measurement does not follow the details of the constant energy surface because this is not perfectly circular. The out-of-plane polarization is zero along the $\bar{\Gamma}\bar{K}$ direction and reaches maxima with opposite sign in the adjacent $\bar{\Gamma}\bar{M}$ directions. That the polarization has to change sign can be understood from the three-fold symmetry of the surface combined with time reversal symmetry; the spin polarization vector has to be opposite for opposite **k**-vectors and on a three-fold symmetric surface a 180° rotation is the same as a 60° rotation. Consequently, the out-of-plane polarization has to become zero in between, i.e. along the $\bar{\Gamma}\bar{K}$ direction.

The measurement shown in figure 6(b) does not intersect the bands of interest, it is therefore not possible to apply the two step fitting routine to this data. The solid line is purely a fit to show the sinusoidal change in polarization. Based solely on this azimuthal dependency of the measured z-polarization, it is not possible to determine what actually happens with the spin polarization vector for different crystal directions. Because the x and y components of the polarization are partly overshadowed by adjacent bands, one could easily conclude that the out-of-plane part of the polarization changes and that the in-plane parts stay the same. This would mean that the length of the polarization vector changes with the crystal direction. However, applying the two step fitting routine of section 4 to a spin resolved MDC measured along the $\bar{\Gamma}\bar{K}$ direction shows that the length of the vector is conserved and that the in-plane components thus slightly increase. This means that the spin polarization vector of the $p_{x,y}$ bands has unit length and rotates in and out of the surface plane with crystallographic orientation, as indicated in the inset of figure 6(b).

The large, and therefore easily detectable spin–orbit effects make Bi/Ag(111) and Pb/Ag(111) ideal model Rashba systems. The detailed verification of theoretical models described above is a nice example of this. The similarity of the atomic structure of both systems, yields an additional free parameter in the study of these systems, namely the intermixing of Pb and Bi. Using spin integrated ARPES Ast and co-workers have found that the band filling and Rashba splitting can be almost linearly tuned by intermixing Pb and Bi on Ag(111) [63]. In LEED or in ARPES no additional periodicity or superposition of the Bi and Pb induced band structures is observed. This indicates that Pb and Bi are not separating into domains and that the intermixing is purely random. The spin resolved measurements on this system, which are reproduced in figures 7(a) and (b) show that, although the splitting is reduced compared to Bi/Ag(111), this additional disorder does not influence the spin structure [64]. Using the vectorial spin analysis routine it was found that the bands are still fully spin polarized and that the polarization vector can still be described by equation (12).

In the $Bi_xPb_{(1-x)}$/Ag(111) mixed surface alloys the band filling can be tuned such that between $x \approx 0.5$ and 0.7 the Fermi level lies between the crossing point of the Rashba split bands and their apex [64]. This region is of special interest because if the simple Rashba model holds, here the density of states (DOS) $\nu(E_F)$ shows a one-dimensional Van Hove singularity $\nu(E_F) \sim (E_0 - E_F)^{-1/2}$ in the limit $E_F \to E_0$, which can also be detected by scanning tunnelling spectroscopy (STS) [65]. Bringing this singularity to the Fermi level is expected to have a profound influence on the electron–phonon interaction [66] and, for relevant systems, on the superconducting transition temperature [67]. Figure 7(b) shows a spin resolved MDC for $Bi_{0.6}Pb_{0.4}$/Ag(111) at the Fermi energy [64], which is cutting exactly through this region. A detailed analysis shows that this data can only be understood by assuming that the spin polarization vectors of the two bands on one side of normal emission are parallel (see inset in figure 7(b)). The simple Rashba model described in section 3 thus holds also for these more complex systems with all the consequences which can be drawn from it.

The unconventional spin texture of two concentric circles with the same spin rotation direction, might naively appear to be an ideal spin filter; all electrons with positive momentum have the same spin, which is opposite to the spin of the electrons with negative momentum. However in particle transport it is the group velocity and not the phase velocity which determines the direction of motion. This group velocity

[1] Note that in [4] the $\bar{\Gamma}\bar{M}$ and the $\bar{\Gamma}\bar{K}$ directions have mistakenly been interchanged.

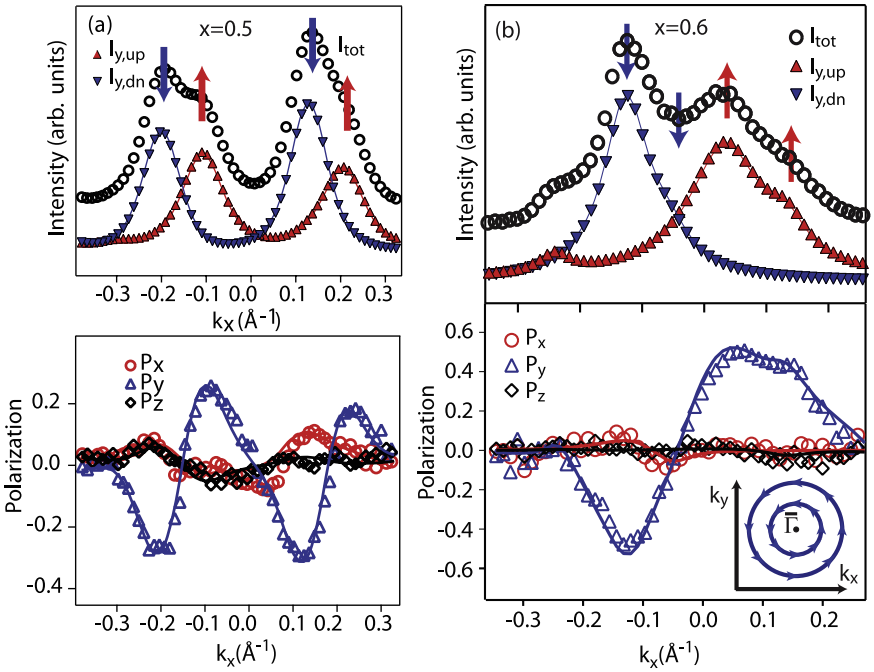

Figure 7. Spin resolved ARPES data of Bi_xPb_{1-x}/Ag(111) for (a) $x = 0.5$ at a binding energy of 0.45 eV and (b) $x = 0.6$ at a binding energy of 50 meV. (top) Total spin integrated intensity (circles) and spin resolved intensity curves projected on the y-axis of a MDC along $\bar{\Gamma}\bar{K}$. (bottom) are the corresponding measured (symbols) and fitted (solid lines) spin polarization data. (Inset in b) Schematically drawn Fermi surface spin texture for $x = 0.6$. (b) is partly from [64].

is, also in this energy range, the same for electrons with opposite spin orientation. The prerequisites for the spin field effect transistor proposed by Datta and Das [33] are therefore present over the full energy range of the bands. One special exception is the situation when the crossing point of the Rashba split bands is exactly at the Fermi level. In this configuration the density of states of the inner branch becomes zero and a significant spin filter effect can be expected [68, 64].

Recently a spin topology with circles with identical spin rotation direction have been predicted for the related long range ordered surface alloy of Bi/Cu(111)($\sqrt{3} \times \sqrt{3}$)R30° [69]. In this system it is predicted that the spin orientation of the unoccupied $p_{x,y}$ states is switched for the inner branch due to hybridization effects. Because these states are unoccupied it is unfortunately not possible to access them with SARPES, but because hybridization is a fundamental effect, the verification of this prediction through SARPES might be possible for related systems.

The surface alloy formed by 1/3 of a monolayer of Sb on Ag(111) is very similar to the Bi/Ag(111) and Pb/Ag(111) surface alloys, but the second layer stacking and the surface corrugation are different [70, 71]. High resolution ARPES measurements on this system could not reveal a splitting of the bands, although theory does suggest that the sp_z bands should show a small splitting [72]. It is currently not clear whether this reduction of the Rashba-type effect is due to the lower spin orbit coupling in the Sb compared to Bi and Pb, or due to the smaller surface corrugation and *hcp* stacking fault. SARPES measurements should be able to measure this splitting and thereby help to elucidate the size of the Rashba effect in Sb/Ag(111).

5.2. Spin splitting of quantum well states in thin metal films

In recent years Rashba-type effects in thin metal films have gained increasing interest, primarily because of the more likely compatibility with technological applications. The reason for this better compatibility is two-fold; firstly, thin metal films can easily be grown on a variety of semiconductor substrates. Large Z materials are in light of the Rashba effect most applicable and Pb and Bi have been grown in atomically flat layers on Si(111) [73, 74]. Pb layers have also successfully been grown on graphene [75], showing a compatibility to the emerging carbon based technology [76]. Secondly, effects occurring in thin metal films are more robust against surface contamination and manipulation than in the previously described surface states.

The electronic structure in thin metal films is dominated by so-called quantum well states (QWS), which are standing electron waves between the substrate/metal interface and the metal/vacuum interface that can form when the film thickness becomes comparable to the electron coherence length [77]. These QWS have been observed with different techniques, ranging from tunnelling conductance and scanning tunnelling spectroscopy to ARPES, in a variety of systems. Because of the dependence of the energy levels on the exact layer thickness, the density of states at the Fermi level also oscillates with thickness. As a result it has been found that many macroscopic properties, such as the growth morphology [78, 79], work function [80], surface reactivity [81], the magnitude and sign of the Hall coefficient [82], and the superconducting transition temperature [83] significantly change when the coverage is increased with just a single monolayer. One can envisage

using this coverage dependence to design systems with the required physical properties, and studying the interaction and inter-dependence of several properties.

In the in-plane direction the QWS typically experience no confinement, and the band structure shows a free electron like dispersion. In a first approximation the QWS can thus similarly to surface states be regarded as a two-dimensional electron gas and the theoretical description for Rashba-type effects given in section 3 can be applied. However, as will be explained below, the situation for QWS is more complex due to the larger spatial extension of the wavefunction and the influence of the substrate. In general, two kinds of spin splitting of QWS in thin metal films can be distinguished; an intrinsic Rashba-type effect similar to what is found for surface states and in semiconductor heterostructures, and alternatively due to interaction with surface or interface states. In order to explore the difference between these two effects we will first discuss the latter.

Using spin integrated ARPES a first suggestion for the spin splitting of QWS was found in Mg on W(110) [84, 85]. Based on the large atomic mass of W, it was argued that the spin orbit interaction occurred at the Mg/W interface and that therefore the splitting decreases as a function of thickness. In a control experiment of Mg on the lighter Mo(110) [86] this interpretation was later refuted and the origin of the band splitting was identified as a hybridization with the substrate surface state, which does not result in spin polarized bands. The possibility of spin split QWS did however stimulate the search for other systems where the states could be spin polarized through interaction with the substrate. For 1 ML of Au on W(110) such a system was found, where the spin polarization of the QWS away from the substrate bands was verified by SARPES [87]. When thin Ag films are grown on the same substrate, the spin splitting of the QWS is very similar to the case of Au films. Taking the much lower atomic mass of Ag compared to Au into account, this clearly indicates that the spin–orbit interaction responsible for the spin splitting in this system, does not occur in the overlayer. If, on the other hand, thin Ag or Au films are grown on a Mo(110) substrate, the QWS show no measurable spin splitting. These permutations of light and heavy substrates and overlayer materials, allow for an insight into the origin of the spin splitting; the authors suggest that a spin dependent hybridization with the spin split substrate states allows the QWS to acquire a spin polarization. As described before, the Rashba parameter can be obtained from the slope of the energy splitting as a function of in-plane momentum. If this analysis is applied to the data for 1 ML of Au on W(110) one obtains a negative Rashba parameter (figure 8(a)), which has no clear physical meaning in this case and cannot be interpreted as a reversal of the spin direction. Moreover, the spin splitting does not seem to disappear at the centre of the SBZ, although this is hard to interpret due to the strong overlap with the substrate bulk bands. This observation supports the notion that for this system the spin splitting is not due to a Rashba-type effect but caused by the interaction with the substrate band structure.

In a follow-up experiment by the same group, on thicker (1–9 ML) Au and Ag films on W(110), it was found that the

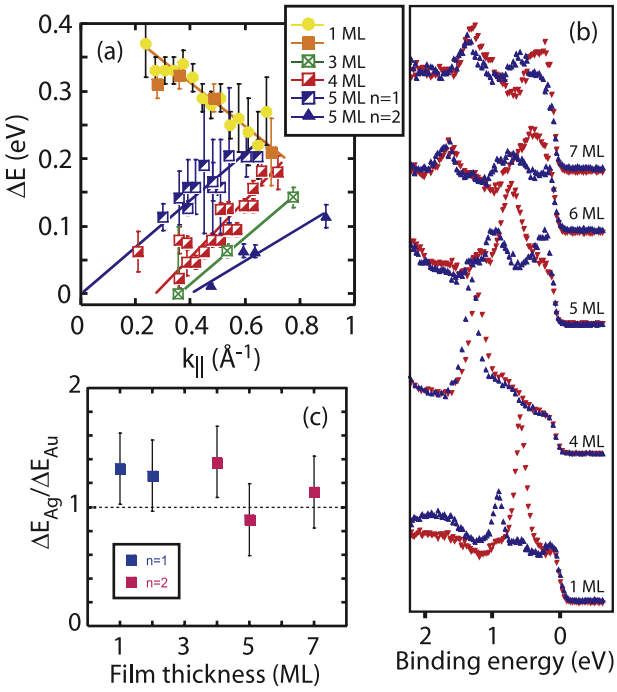

Figure 8. (a) Energy splitting in Au QWS on W(110) as a function of $k_\parallel$ and coverage. (b) Spin resolved spectra for several coverages of Au on W(110) at $-7°$ of normal emission, obtained at $h\nu = 50$ eV. (c) Ratio of the energy splitting in Ag and Au QWS on W(110) as a function of coverage. Reproduced with permission from [88]. Copyright 2008 by the American Physical Society.

spin splitting of the QWS can also be observed for coverages larger than 1 ML [88], see figure 8(b). For the presented data there seems to be no clear dependence of the spin splitting on the coverage; the splitting of the highest occupied QWS of a 4 ML thick film is smaller than for the 1 or 5 ML thick films. Furthermore the splitting for the Ag QWS is slightly larger than for the Au QWS for almost all coverages, as shown in figure 8(c), which refutes an explanation of the spin splitting by a Rashba-type effect in the film itself. In contrast to the results for the single ML of Au or Ag on W(110) the Rashba parameter is positive for the thicker films, as shown in figure 8(a). A linear extrapolation of the band splitting to $k_\parallel = 0$ yield for most QWS a negative splitting, which cannot be explained by a Rashba-type effect where the splitting should go to zero. The authors explain the spin polarization of the QWS by the Bragg reflection at the interface. It is argued that similarly to the situation in spin polarized LEED [9], the electrons obtain a spin polarization due to the reflection of the W(110) substrate, this polarization is then enhanced due to the multiple scattering events that the electrons experience in the quantum cavity. This can be interpreted as a spin dependent hybridization of the QWS with the band structure of the substrate. A close examination of the spin resolved spectra indicates that the spin splitting vanishes when the QWS cross the surface-projected W(110) band gap; i.e. the QWS are only spin split when they are inside this gap. It would be interesting to plot the band splitting as a function of $k_\parallel$ and binding energy and thus indirectly as a function of the distance to the projected band edge, since the data seem to indicate that the splitting is largest when the QWS is furthest away from this edge. It would

therefore seem reasonable that similarly as for a single ML of Au or Ag, the spin splitting in Au and Ag QWS on W(110) can be explained through a hybridization with the surface states of the substrate.

A strong hybridization between QWS and surface states has also been observed by spin integrated ARPES for a $\sqrt{3} \times \sqrt{3}$ reconstruction of Bi on thin Ag layers on Si(111) [89, 90], although the result of this hybridization is different. The crystal and electronic structure of the surface are very similar to the surface alloys described in section 5.1, including the Rashba-type spin splitting of the bands. Unlike for the previously described surface alloys, the $\sqrt{3} \times \sqrt{3}$ reconstruction is not formed on a bulk Ag(111) crystal, but on thin Ag films grown on Si(111). These thin films contain well defined QWS with a free electron like character [91]. At the crossing points of the upward dispersing QWS and the downward dispersing surface alloy deduced surface states, the bands can hybridize and gaps open up. This effect is similar to what has been observed at the crossing point of QWS and substrate bands in Al/Si(111) [92] and other systems. However, since the surface states are spin polarized, only the electrons in the QWS with the same spin direction can hybridize with them. The other spin direction will not be affected and the bands continue in the hybridization gap. This results in a momentum and energy dependent spin polarization of the QWS. Since the binding energy of the QWS can be varied through the exact layer thickness, the energy and in-plane momentum of the spin gaps can also be varied accordingly. At the moment no SARPES data has been published of this system that can verify these observations, partly due to the required high energy and angle resolution also in spin resolved mode.

In the systems described above, the spin polarization in non-magnetic thin metal films is due to an interaction between the QWS and the surface or interface states. Let us now turn to systems where a Rashba-type effect and the corresponding spin–orbit coupling occur in the thin films itself. Just as surface states, QWS are standing waves confined between the substrate and the image potential that have a free electron like in-plane dispersion. In some models QWS are therefore regarded as surface states in the bulk of the film, or surface states are regarded as zero thickness QWS [27, 93]. One would therefore expect that for an asymmetric quantum well, such as is typically the case for realistic systems, the QWS would show a Rashba-type spin splitting. Using spin integrated ARPES no spin splitting has been found for QWS in Pb [73, 94, 95, 75] and Bi [74] layers, where due to the high atomic mass the splitting is expected to be sizeable. As a reason for the absence of this spin splitting, it was suggested that the charge density in the QWS is located too far away from the surface or interface to experience the potential gradient [74, 96] or to the idea that QWS are standing waves and that therefore a similar argument as for the fact that it not possible to observe a Rashba effect with scanning tunnelling spectroscopy should apply [30]. Recent SARPES measurements on QWS in thin Bi films show that the spin polarization of the surface states is reduced when they transform into QWS close to the zone boundary [53]. Simultaneously the charge is distributed further away from the borders of the film. This seems to support the first explanation, although the spin resolution in [53] is rather limited because of the type of Mott detector which is used as is discussed in section 2. The second explanation cannot be entirely correct because surface states are also standing waves in the direction perpendicular to the surface and here clear spin splittings have been observed. The argumentation of Petersen and Hedegård [30] only applies to standing waves along the k-direction where also the momentum splitting should occur.

However, a more likely reason that no spin split QWS were observed in these experiments is due to the fact that the splitting is too small to be measured with high resolution spin integrated ARPES, and that also in a spin resolved measurement one needs very high spin resolution. In figure 9 SARPES spectra for 8 and 10 ML thick Pb films on Si(111) are shown [5]. Characteristic for this system are the almost perfect layer-by-layer growth at low temperatures [95] and the high effective mass of the QWS around the zone centre [97], which can be explained by a reduced overlap of the $6p_z$ orbitals [98]. In the polarization curves of figures 9(a) and (b), a polarization signal can be observed with a magnitude of less than 10%. It should be noted that this is clearly within the statistical noise of [53], which would explain why no spin splitting of the Bi QWS is observed in this work. Using the two step analysis routine described in section 4, one can fit the data with two fully polarized bands with opposite spin polarization vectors. At $k_y = -0.08$ Å^{-1} the splitting between the two bands is 12 meV for the 8 ML thick film. The exact binding energy of a QWS depends on the local boundary conditions [99]. It is therefore fair to assume that the intrinsic linewidth of the QWS will not be below 20 meV, and thus larger as the splitting. This means that even with perfect instrumental resolution and without thermal broadening it will not be possible to resolve the two spin split lines in spin integrated ARPES.

As can be seen in the series of polarization spectra in figure 9(c), the splitting disappears and then changes sign when going through the centre of the SBZ, as is expected from an intrinsic Rashba-type spin–orbit splitting. Correspondingly the deduced energy difference of the QWS shows a linear dependence on $k_\parallel$ and goes to zero when $k_\parallel = 0$.

From equation (10) for a Rashba system it can be deduced that

$$\alpha_R = \frac{E_+(\boldsymbol{k}) - E_-(\boldsymbol{k})}{2\boldsymbol{k}}. \tag{15}$$

The Rashba parameter can thus be obtained by taking half the slope of the energy splitting versus in-plane momentum. This yields a value of $\alpha_R = 0.04 \pm 0.005$ eV Å for the 10 ML thick Pb film. This is comparable to the value of 0.07 eV Å found for the Rashba effect in InGaAs/InAlAs heterostructures [35], but smaller than the value of 0.33 eV Å for the Au(111) surface state [39]. The momentum splitting obtained from this value is $k_0 = 0.035 \pm 0.002$ Å^{-1}, compared to 0.012 Å^{-1} for the semiconductor heterostructures and 0.028 Å^{-1} for Au(111). This means that although the Rashba parameter in thin Pb films on Si(111) is small compared to the surface states discussed in sections 3 and 5.1, the momentum splitting is large enough to have technological relevance.

Apart from being the first observation of an intrinsic Rashba-type effect in metallic QWS, there are two more

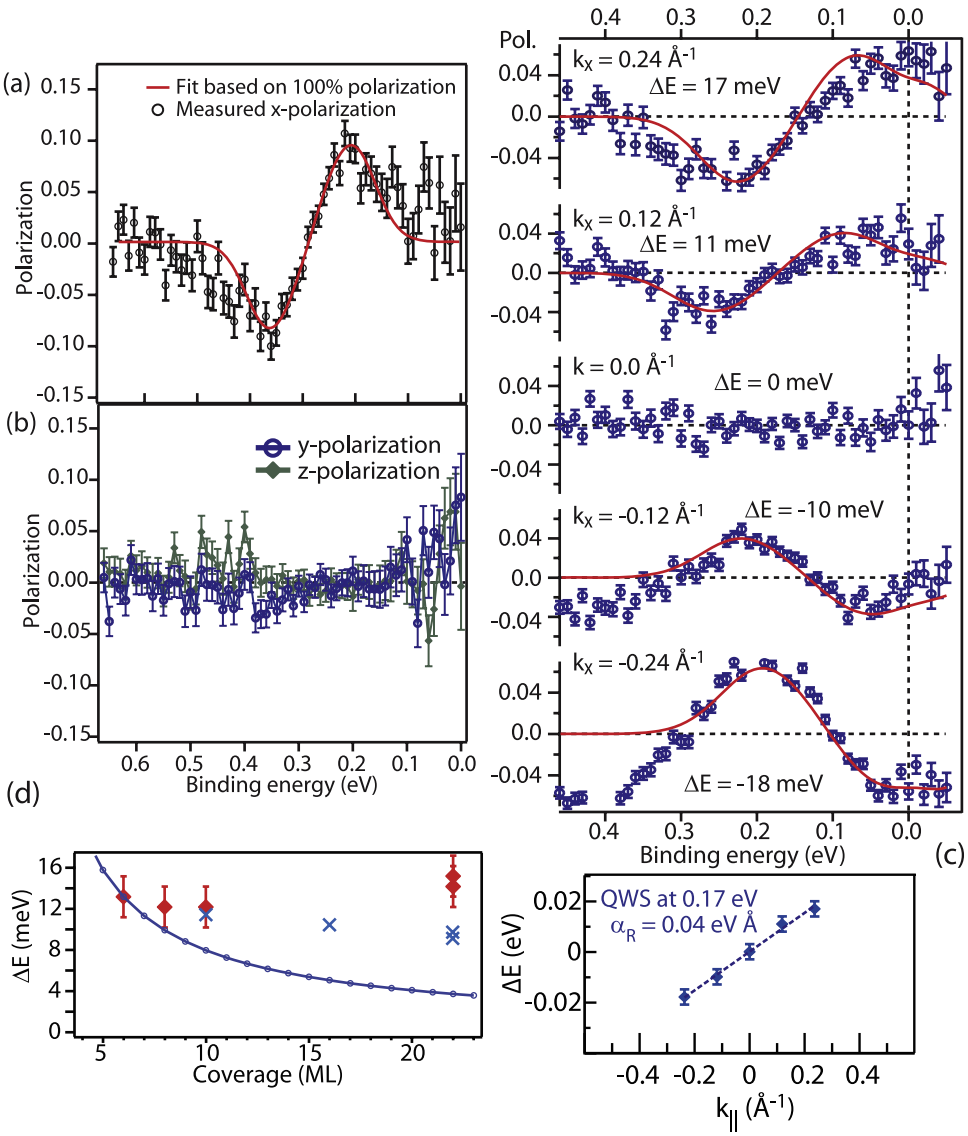

Figure 9. (a) and (b) SARPES data for an 8 ML thick Pb layer on Si(111)$\sqrt{3}$ at $k_y = -0.08$ Å^{-1} and $k_x = 0$. (a) Measured (open circles) and modelled (solid line) spin polarization in the x-direction of the sample. (b) Measured spin polarization along the y (blue circles) and z (green diamonds) direction of the sample. (c) Measured (symbols) and fitted (solid line) polarization spectra for a 10 ML thick Pb film at $k_y = 0$. The lower panel plots the energy splitting as a function of k_x. (d) Measured (red diamonds) and calculated (blue crosses) spin splitting as function of coverage at $k_y = -0.08$ Å^{-1} and $k_x = 0$, the blue circles show the intuitively expected 1/thickness dependence. Reproduced with permission from [5]. Copyright 2008 by the American Physical Society.

striking results for the spin splitting of QWS in Pb/Si(111). The first is that the magnitude of the splitting shows no strong dependence on the layer thickness for coverages at least up to 22 ML. As can be seen in figure 9(d) the band splitting at $\mathbf{k} \approx 0.1$ Å^{-1} varies between 11 and 15 meV for coverages between 6 and 22 ML, and shows no clear decaying trend as a function of coverage. Furthermore, the spin direction is reversed compared to the Au(111) surface state. Both of these unconventional observations can be explained through the origin of the Rashba-type spin–orbit splitting in the Pb films.

The integral of the wavefunction throughout the quantum well has to sum up to unity, which means that the amplitude of the wavefunction decreases as a function of coverage. If for the Rashba Hamiltonian the amplitude of the wavefunction decreases, this means that also the spin splitting will decrease. If the spin splitting of Pb QWS were purely an effect occurring at the interfaces, the spin splitting would decrease inversely proportional to the thickness. As will be explained below, the spin–orbit interaction occurs throughout the layer and the measured spin splitting is the nett effect integrated over the full thickness which can compensate the decrease in amplitude of the wavefunction.

On a microscopic scale the Rashba effect can be understood through the local distribution of the wavefunction around an atom and the non-zero $l \cdot s$ coupling resulting from this [52]. For a propagating wave the temporal average of this spin–orbit coupling is zero and therefore the Rashba effect can only be observed for standing waves such as for example surface states. As explained above, QWS can be regarded

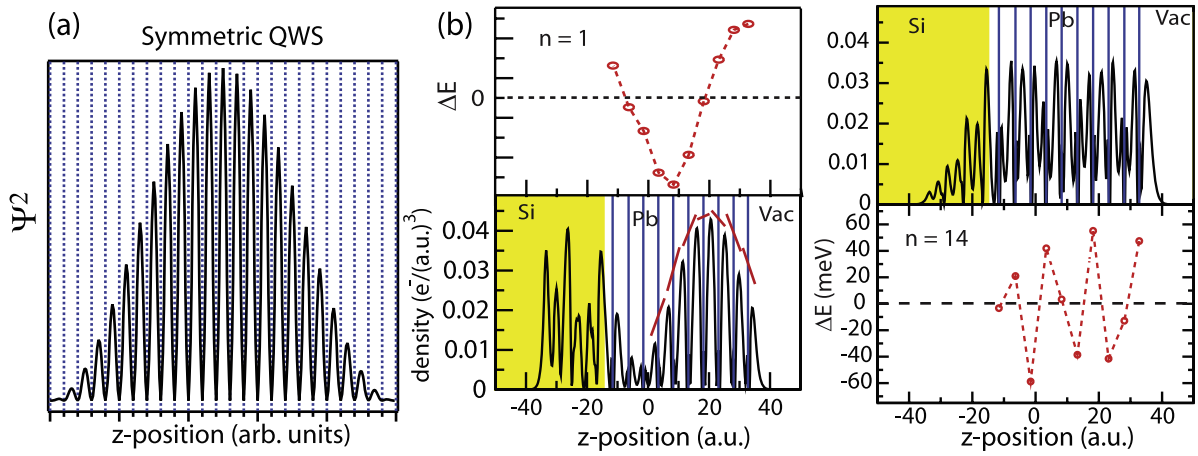

Figure 10. (a) Wavefunction distribution for a symmetric quantum well state with quantum number $n = 1$. (b) Wavefunction distribution calculated for $n = 1$ and 14 QWS in Pb on Si(111) at $k = 0.1\bar{\Gamma}\bar{K}$ and the local Rashba effect at each atomic layer. The blue lines indicate the position of the atomic planes.

as standing electron waves between the two boundaries of the film. In the case of symmetric boundary conditions the wavefunction inside the quantum well will look like figure 10(a). One can see that around most Pb atoms the wavefunction distribution is not symmetric and one obtains a local Rashba effect. On the other hand, due to the symmetry of the complete wavefunction in the well, there is always the exact opposite situation on the other side of the well, producing en equal but opposite local Rashba effect. In a photoemission experiment one measures the sum of all these effects which in this case will be zero.

For many systems and also for the Pb films discussed here, the two boundaries of the quantum well are not the same and the wavefunction will penetrate the two boundaries to a different extent. As a result the mirror symmetry of the wavefunction around the centre of the layer is lost and the local Rashba effects no longer cancel. In figure 10(b) the calculated wavefunction and the resulting local Rashba splitting are shown for the $n = 1$ and 14 QWS in a 10 ML thick Pb film on Si(111) at $k_{\parallel} = 0.1$ Å^{-1}. This local Rashba splitting for each layer has been calculated by turning the spin–orbit interaction off for all other layers. Due to the reciprocal influence of the spin–orbit coupling on the exact shape of the wavefunction this is of course not a very exact method and the net Rashba effect obtained by adding all the local Rashba effects does not necessarily correspond to what is found when considering the full system. One does, however, directly see the oscillations in the spin splitting for each layer and the loss of mirror symmetry around the centre of the layer.

The small measured spin splitting can be explained as a result of these competing effects, in contrast to the situation for a single crystal surface state where the contributions of the top layers all have the same sign. Similarly one can understand the change in spin direction compared to single crystal surface states as a nett shift of the wavefunction towards the substrate; i.e. the phase shift at the Pb/Si interface is larger than at the Pb/vacuum interface. This means that in principle a control of the spin splitting and direction can be achieved through a variation of the phase shift at the metal/substrate interface [100, 101].

To conclude, the small spin splitting, the change in spin direction and the constant spin splitting as a function of coverage for Pb QWS on Si(111) can be explained through a careful analysis of the local wavefunction asymmetries and the resulting spin–orbit coupling.

5.3. Spin effects in graphene and topological metals

Graphene, a single layer of graphite, has recently attracted a lot of attention because of its potential applications for a new generation of electronics [102]. Further it has been suggested that spin effects might play an important role in graphene [103], although later it has been suggested that the intrinsic spin–orbit coupling in graphene might be too small to measure any such effects [104]. Given the unique electronic properties of graphene, it is of interest to induce a spin splitting of the bands.

Using spin integrated ARPES a shift of 225 meV of the graphene π-band binding energy was found for different magnetization directions in epitaxial graphene on Ni(111) [105]. This shift has been attributed to a Rashba-type spin–orbit coupling which becomes visible also in spin integrated ARPES due to the exchange splitting in the Ni(111) substrate. SARPES measurements on the same system could not verify a Rashba-type effect with similar magnitude or above the detection limit of about 50 meV [106]. Also in the related system of graphene on Co(111) a spin polarization of the graphene π-bands could not be observed [106]. It should be noted that due to the limited resolution in these experiments, it is not possible to say whether a small spin splitting might be present or not. The large energy shift reported in [105] however seems not to be due to a Rashba-type effect and its origin remains unclear.

Although a spin splitting in graphene grown on ferromagnetic substrates has so far not been verified by SARPES, a small Rashba-type effect has been reported in quasi-free-standing graphene on a monolayer of Au on

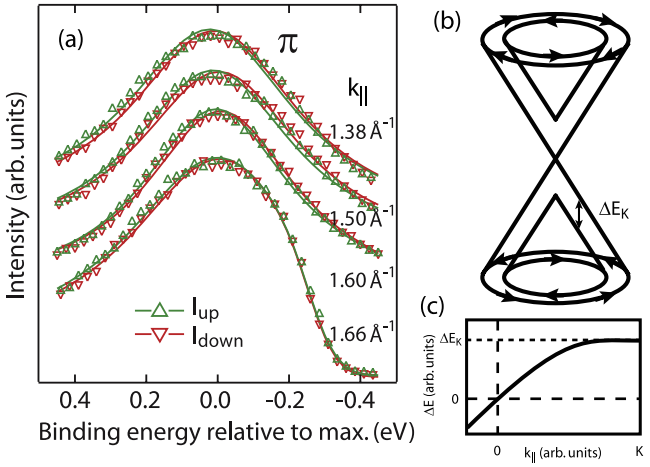

Figure 11. (a) Spin resolved spectra for Au intercalated graphene/Ni(111) obtained at different $k_{\|}$. The spectra are aligned in momentum to their maxima. From [107]. (b) Proposed spin resolved band structure of graphene around the K-point. (c) Proposed dependency of the Rashba energy splitting as a function of momentum for graphene.

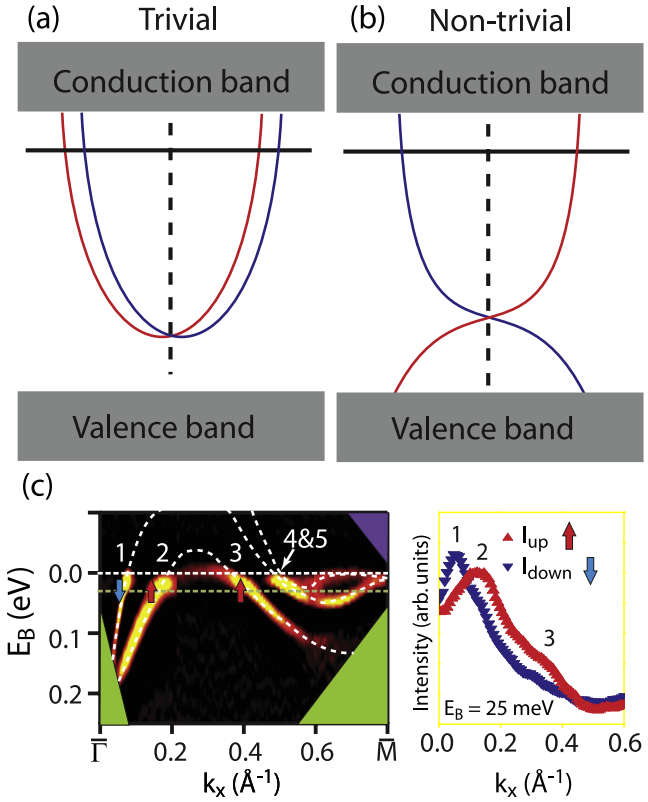

Figure 12. (a) Trivial topology of spin split surface states such as for example for Au(111), with an even number of Fermi level crossings. (b) Non-trivial topology of a topological metal or insulator with an odd number of Fermi level crossings. (c) Band structure of $Bi_{0.9}Sb_{0.1}$(111) with five Fermi level crossings and a spin resolved MDC projected on the y-axis obtained at a binding energy of 25 meV. The green and purple areas represent the bulk valence and conduction band, respectively. Reproduced with permission from [50]. Copyright 2009 AAAS.

Ni(111) [107]. This data is reproduced in figure 11(a), the splitting is only 13 meV and is hardly visible above the measurement noise. A clear dependence of the splitting on the in-plane momentum can therefore not be distinguished. Keeping in mind that the K-point is not a time reversal protected point, and the bands therefore do not have to become degenerate here, the result of a Rashba-type spin splitting could look like what is shown in figure 11(b). Note that the gap opening suggested here is markedly different from the case of bilayer graphene [108], in the latter case the bands are still degenerate. Although at first instance it seems like a gap has opened up for only one spin direction, which would make graphene magnetic, this is not the case; both spin directions are still in balance at the Fermi level. In this case the energy splitting of the bands would show a behaviour as sketched in figure 11(c) as a function of in-plane momentum. Around the bottom of the band the band splitting increases linearly and levels off around the Fermi level at a value determined by the slope of the bands and the momentum spacing. Given the fact that these states are located around the K-point, spin frustration effects could occur, such as recently reported for Tl/Si(111) [34]. Measurements to determine the exact spin orientation around the K-point in graphene are on the verge of what is possible nowadays with spin resolved ARPES.

In most of the systems described above, the Rashba effect resulted in a pair of bands that either both cross the Fermi level or both are fully (un)occupied, an example of this trivial topology is given in figure 12(a). If the surface states with different spin directions recombine with either the occupied or unoccupied part of the bulk band structure, the number of surface states crossing the Fermi level will change and the topology will become non-trivial. In figure 12(b) this is illustrated for the situation where the spin up band connects to the bulk bands below the Fermi level and the spin down band above the Fermi level. As a result there will be an odd number of spin polarized Fermi level crossings on a straight line between $\bar{\Gamma}$ and the next time reversal invariant momentum. This means that there is an odd number of spin channels for a given momentum direction. Given the fact that time inversion symmetry still holds, the surface thus supports channels with opposite spin going in opposite directions, and no channels with opposite spin orientation going in the same direction. Therefore an electron would have to flip its spin when it changes direction, which is very unlikely in the absence of magnetic impurities. As a result, the conductance is hardly influenced by non-magnetic impurities and one could expect a very efficient spin transport. The graphene band structure in figure 11(b) is an example of this situation where only one pair of spin polarized bands crosses the Fermi level. Many of the ideas described below had therefore initially been described for graphene [103].

The situation described above with an odd number of Fermi crossings between $\bar{\Gamma}$ and the next TRIM is termed a topological metal [109, 110]. If this topological metal forms the surface of an insulator, the whole system is called a topological insulator which in turn forms the basis of the recently discovered quantum spin Hall effect [111]. A complete description of this effect goes beyond the scope of this review and here the presented heuristic description should

suffice. In order to determine whether a sample has the Fermi surface topology required for the quantum spin Hall effect and can thus accommodate dissipationless spin currents without applying a magnetic field, spin and angle resolved photoemission is currently the best method. In the following examples SARPES has been successfully used to show that the surface of the system is a topological metal.

The band structure of $Bi_{0.9}Sb_{0.1}$(111) shown in figure 12(c) on first sight strongly resembles the band structure of pure Bi(111), there is however one major difference that has far reaching consequences. Due to the alloying with Sb a gap is opened up around the Fermi level, making the bulk insulating. Because the surface states with different spin directions connect to either the occupied or unoccupied bulk bands, the number of Fermi crossings must become odd. Here it should be noted that spin degenerate states should be counted twice (once for spin up, once for spin down) and that the verification of the spin structure is thus of crucial importance. The spin resolved data clearly indicate that all surface state bands are spin polarized and that $Bi_{0.9}Sb_{0.1}$(111) forms a quantum spin Hall system [50].

Due to the small band gap of only 50 meV and the large number of spin polarized bands crossing the Fermi level, $Bi_{0.9}Sb_{0.1}$(111) is a relatively weak topological insulator. Recently a new class of materials around Bi_2Se_3 and Bi_2Te_3 has been found with a band gap of about 0.3 eV and only a single spin polarized state crossing the Fermi level [112, 113]. The spin structure has also been verified by SARPES measurements and it has been found that by systematic hole-doping with Ca and NO_2 the Dirac point (crossing point of the bands) can be placed exactly at the Fermi level [114]. This can open up a whole new realm of physics, including fault-tolerant quantum computing through the realization of Majorana fermions [115, 116].

In $Bi_{0.9}Sb_{0.1}$(111) and Bi_2Se_3 the electrons of the surface state can move in the full two-dimensional plane of the surface, where their direction of motion is determined by their spin. In principle the non-trivial edge states required for the quantum spin Hall phase can be found on the N-dimensional border of a $N + 1$-dimensional topological insulator. The most promising pathway to find a one-dimensional quantum spin Hall phase would therefore seem to look at the edges of two-dimensional systems. Although in a theoretical approach it is relatively easy to handle two-dimensional systems, it is hardly feasible in an photoemission experiment. On the other hand can the surface states of vicinal samples show a strong one-dimensional behaviour [117–119]. This opens up the possibility to look at the one-dimensional edge states of a three-dimensional system.

As has been shown before, pure Bi has in many aspects a very similar Fermi surface to the topological insulators which are derived from it. Therefore results obtained for the surface states on pure Bi vicinal surfaces can be transferred to the surface states of vicinal topological insulators. Bi(114) forms a prime example of a one-dimensional surface on a three-dimensional bulk system. The surface consists of an 56° miscut of the Bi(111) surface which, together with a (1×2) reconstruction, results in one-dimensional rows of atoms separated by 14.2 Å [120]. Apart from the zig-zag structure of the bulk bands, the Fermi surface consists of straight parallel lines perpendicular to the steps as shown in figure 13(a). In this high resolution ARPES data the surface state appears as a single line although all other bismuth surfaces are characterized by a large spin splitting of the surface states [40]. The spin resolved data in figures 13(b) and (c) clearly shows that this single line actually consists of two states with opposite spin directions. Using the two step analysis routine described in section 4 it is possible to accurately extract the spin polarization vectors of these states, which are found to be tangential to the constant energy contours. Due to the large step density it is found that the polarization vectors have a relatively large out-of-plane component of 30°. Furthermore the spin polarization does not depend on where along the lines the measurement is performed, which confirms the one-dimensional character of the states; for two-dimensional states one would expect that the spin polarization vector would primarily lie on a circle centred around $\bar{\Gamma}$. Within one surface Brillouin zone, each spin direction crosses the Fermi energy once, which clearly indicates that the surface of Bi(114) is a topological metal. It can therefore be expected that $Bi_{0.9}Sb_{0.1}$(114) forms a topological insulator with one-dimensional edge states and is thus a good candidate for the observation of a one-dimensional quantum spin Hall effect on surfaces.

Figure 13(d) shows a schematic comparison between Au(111) which is the prime example of a topologically not protected two-dimensional spin split surface state, and Bi(114). As indicated above, the main difference is of course the number of Fermi crossings. For Bi the outer branch of the surface state bends down again and hybridizes with the bulk bands at higher binding energy. It should be noted that although the topology is totally different, the spin orientation of the Au(111) and Bi(114) surface states is the same. This is directly related to the Rashba effect being the origin of the spin splitting in both cases. Unlike for the quantum well states in section 5.2 there are no competing effects here and the only potential gradient is due to the surface of the sample. A reversal of the spin direction for a topological insulator would open up a new field of physics and can be regarded as the condensed matter equivalent of right-handed neutrinos. Up to now only two cases of spin reversal are known, namely for one magnetization direction in oxygen on Gd(0001) [121] and for Pb quantum well states on Si(111) [5]. Both of these systems are topologically trivial and thus not relevant for the quantum spin Hall effect themselves, but the obtained detailed understanding of this spin reversal can certainly help in the conception of a right-handed topological insulator.

6. Conclusions

In many instances spin resolved ARPES follows the results of spin integrated ARPES, which is mainly caused by the fact that spin integrated experiments are faster and easier. However, the information which is obtained with SARPES is often much richer and allows for a deeper insight into many basic physical phenomena. Furthermore, in some instances even ARPES

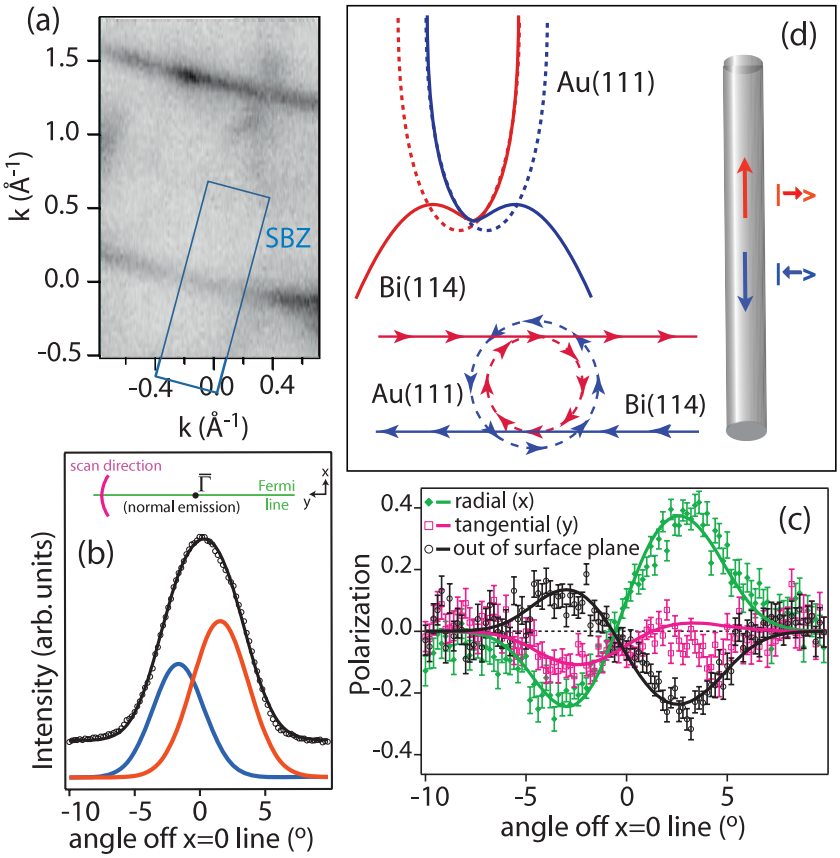

Figure 13. (a) Fermi surface of Bi(114) obtained at a photon energy of 70 eV. The rectangle indicates the surface Brillouin zone. (b) Spin integrated intensity (black markers) measured across the surface state in (a) and the spin resolved components (solid lines) along the quantization axis determined from the vectorial analysis. (c) Measured (markers) and fitted (lines) spin polarization data for the scan across the one-dimensional surface state. (d) Comparison between the trivial surface states of Au(111) and the non-trivial surface states of Bi(114), and a summary of the one-dimensional spin separation on the surface of Bi(114). Reproduced with permission from [120]. Copyright 2009 by the American Physical Society.

experiments with the highest available resolution cannot compete with SARPES experiments in resolving features with different spin orientations. Given the additional spin tag, spin and angle resolved photoemission will continue to emerge as a powerful tool for the detection of novel spin phenomena in magnetic and non-magnetic materials.

Acknowledgments

I am indebted to Jürg Osterwalder for his continuous support and guidance. Jorge Lobo-Checa introduced me to the fine details of spin and angle resolved photoemission and I am grateful for his contribution to make COPHEE a competitive SARPES instrument. Fabian Meier has been involved in most measurements at COPHEE and has developed the vectorial analysis routine, I thank him for this and his constructive input. Gustav Bihlmayer, Jürgen Henk and Christopher Mudry have helped me in understanding much of the theoretical background of the Rashba effect. I thank Christian Ast for stimulating discussions about the surface alloys and Oliver Rader for providing some figures.

Many of the experiments described in this review have been performed at the COPHEE end station at the Surface and Interface Spectroscopy beamline at the Swiss Light Source which has been designed and built by Moritz Hoesch. This would not have been possible without the great team of people that assisted in constructing and commissioning the machine, and I would like to thank Vladimir Petrov, Matthias Muntwiler, Matthias Hengsberger, Taichi Okuda, Thomas Greber, Luc Patthey, Werner Deichmann, Fritz Dubi, Christoph Hess and Martin Klöckner for their knowledge, time and effort. This work has been supported by the Swiss National Science Foundation.

References

[1] Wolf S A, Awschalom D D, Buhrman R A, Daughton J M, von Molnar S, Roukes M L, Chtchelkanova A Y and Treger D M 2001 Spintronics: a spin-based electronics vision for the future *Science* **294** 1488–95

[2] Kohda M, Bergsten T and Nitta J 2008 Manipulating spin–orbit interaction in semiconductors *J. Phys. Soc. Japan* **77** 031008

[3] LaShell S, McDougall B A and Jensen E 1996 Spin splitting of an Au(111) surface state band observed with angle resolved photoelectron spectroscopy *Phys. Rev. Lett.* **77** 3419–22

[4] Meier F, Dil H, Lobo-Checa J, Patthey L and Osterwalder J 2008 Quantitative vectorial spin analysis in angle-resolved photoemission: Bi/Ag(111) and Pb/Ag(111) *Phys. Rev.* B **77** 165431

[5] Dil J H, Meier F, Lobo-Checa J, Patthey L, Bihlmayer G and Osterwalder J 2008 Rashba-type spin–orbit splitting of quantum well states in ultrathin Pb films *Phys. Rev. Lett.* **101** 266802

[6] Hüfner S 2003 *Photoelectron Spectroscopy: Principles and Applications* 3rd edn (Berlin: Springer)

[7] Mott N F 1929 The scattering of fast electrons by atomic nuclei *Proc. R. Soc.* A **124** 425–2

[8] Kessler J 1985 *Polarized Electrons* 2nd edn (Berlin: Springer)

[9] Kirschner J and Feder R 1979 Spin polarization in double diffraction of low-energy electrons from W(001): experiment and theory *Phys. Rev. Lett.* **42** 1008–11

[10] Thiel R, Tillmann D and Kisker E 1989 Very-low-energy spin-polarized electron diffraction from Fe(001) *Z. Phys.* B **77** 1

[11] Bertacco R, Onofrio D and Ciccacci F 1999 A novel electron spin-polarization detector with very large analyzing power *Rev. Sci. Instrum.* **70** 3572–6

[12] Winkelmann A, Hartung D, Engelhard H, Chiang C-T and Kirschner J 2008 High efficiency electron spin polarization analyzer based on exchange scattering at Fe/W(001) *Rev. Sci. Instrum.* **79** 083303

[13] Okuda T, Takeichi Y, Maeda Y, Harasawa A, Matsuda I, Kinoshita T and Kakizaki A 2008 A new spin-polarized photoemission spectrometer with very high efficiency and energy resolution *Rev. Sci. Instrum.* **79** 123117

[14] Lebedev G, Jozwiak C, Andresen N, Lanzara A and Hussain Z 2008 Tof electron energy analyzer for spin and angular resolved photoemission spectroscopy *CPO-7: Proc. 7th Int. Conf. on Charged Particle Optics*; *Phys. Proc.* **1** 413–23

[15] Sherman N 1956 Coulomb scattering of relativistic electrons by point nuclei *Phys. Rev.* **103** 1601–7

[16] Hoesch M 2002 Spin-resolved Fermi surface mapping *PhD Thesis* Universität Zürich

[17] Hoesch M, Greber T, Petrov V N, Muntwiler M, Hengsberger M, Auwaerter W and Osterwalder J 2002 Spin-polarized Fermi surface mapping *J. Electron Spectrosc. Relat. Phenom.* **124** 263–79

[18] Nelson D F and Pidd R W 1959 Measurement of the Mott asymmetry in double scattering of electrons *Phys. Rev.* **114** 728–35

[19] Petrov V N, Grebenshikov V V, Grachev B D and Kamochkin A S 2003 New compact classical 40 kV Mott polarimeter *Rev. Sci. Instrum.* **74** 1278–81

[20] Petrov V N, Grebenshikov V V, Andronov A N, Gabdullin P G and Maslevtcov A V 2007 Ultrafast compact classical Mott polarimeter *Rev. Sci. Instrum.* **78** 025102

[21] Gray L G, Hart M W, Dunning F B and Walters G K 1984 Simple, compact, medium-energy Mott polarization analyzer *Rev. Sci. Instrum.* **55** 88–91

[22] Petrov V N, Galaktionov M S and Kamochkin A S 2001 Comparative tests of conventional and retarding-potential Mott polarimeters *Rev. Sci. Instrum.* **72** 3728–30

[23] Lüth H 2001 *Solid Surfaces, Interfaces and Thin Films* 4th edn (Berlin: Springer)

[24] Grønlund F and Højlund Nielsen P E 1972 The 5 × 20 surface structure of gold *J. Appl. Phys.* **43** 3919–21

[25] Perdereau J, Biberian J P and Rhead G E 1974 Adsorption and surface alloying of lead monolayers on (111) and (110) faces of gold *J. Phys. F: Met. Phys.* **4** 798–806

[26] Van Hove M A, Koestner R J, Stair P C, Bibérian J P, Kesmodel L L, BartoS I and Somorjai G A 1981 The surface reconstructions of the (100) crystal faces of iridium, platinum and gold: I. Experimental observations and possible structural models *Surf. Sci.* **103** 189–217

[27] Echenique P M and Pendry J B 1978 The existence and detection of Rydberg states at surfaces *J. Phys. C: Solid State Phys.* **11** 2065–75

[28] Rashba É I 1960 Properties of semiconductors with an extremum loop i. Cyclotron and combinational resonance in a magnetic field perpendicular to the plane of the loop *Sov. Phys.—Solid State* **2** 1109

[29] Bychkov Yu A and Rashba E I 1984 Oscillatory effects and the magnetic susceptibility of carriers in inversion layers *J. Phys. C: Solid State Phys.* **17** 6039–45

[30] Petersen L and Hedegård P 2000 A simple tight-binding model of spin–orbit splitting of sp-derived surface states *Surf. Sci.* **459** 49–56

[31] Winkler R 2003 *Spin-Orbit Coupling Effects in Two-Dimensional Electron and Hole Systems* (*Springer Tracts in Modern Physics*) (Berlin: Springer)

[32] Henk J, Hoesch M, Osterwalder J, Ernst A and Bruno P 2004 Spin–orbit coupling in the L-gap surface states of Au(111): spin-resolved photoemission experiments and first-principles calculations *J. Phys.: Condens. Matter* **16** 7581–97

[33] Datta S and Das B 1990 Electronic analog of the electro-optic modulator *Appl. Phys. Lett.* **56** 665–7

[34] Sakamoto K *et al* 2009 Abrupt rotation of the Rashba spin to the direction perpendicular to the surface *Phys. Rev. Lett.* **102** 096805

[35] Nitta J, Akazaki T, Takayanagi H and Enoki T 1997 Gate control of spin–orbit interaction in an inverted $In_{0.53}Ga_{0.47}As/In_{0.52}Al_{0.48}As$ heterostructure *Phys. Rev. Lett.* **78** 1335–8

[36] Harten U, Lahee A M, Peter Toennies J and Wöll Ch 1985 Observation of a soliton reconstruction of Au(111) by high-resolution helium-atom diffraction *Phys. Rev. Lett.* **54** 2619–22

[37] Rotenberg E, Chung J W and Kevan S D 1999 Spin–orbit coupling induced surface band splitting in Li/W(110) and Li/Mo(110) *Phys. Rev. Lett.* **82** 4066–9

[38] Hochstrasser M, Tobin J G, Rotenberg E and Kevan S D 2002 Spin-resolved photoemission of surface states of W(110) − (1 × 1)H *Phys. Rev. Lett.* **89** 216802

[39] Hoesch M, Muntwiler M, Petrov V N, Hengsberger M, Patthey L, Shi M, Falub M, Greber T and Osterwalder J 2004 Spin structure of the shockley surface state on Au(111) *Phys. Rev.* B **69** 241401

[40] Hofmann Ph 2006 The surfaces of bismuth: structural and electronic properties *Prog. Surf. Sci.* **81** 191–245

[41] Hengsberger M, Segovia P, Garnier M, Purdie D and Baer Y 2000 Photoemission study of the carrier bands in Bi(111) *Eur. Phys. J.* B **17** 603–8

[42] Ast C R and Höchst H 2001 Fermi surface of Bi(111) measured by photoemission spectroscopy *Phys. Rev. Lett.* **87** 177602

[43] Ast C R and Höchst H 2003 Indication of charge-density-wave formation in Bi(111) *Phys. Rev. Lett.* **90** 016403

[44] Agergaard S, Sondergaard Ch, Li H, Nielsen M B, Hoffmann S V, Li Z and Hofmann Ph 2001 The effect of reduced dimensionality on a semimetal: the electronic structure of the Bi(110) surface *New J. Phys.* **3** 15

[45] Koroteev Yu M, Bihlmayer G, Gayone J E, Chulkov E V, Blügel S, Echenique P M and Hofmann Ph 2004 Strong spin–orbit splitting on Bi surfaces *Phys. Rev. Lett.* **93** 046403

[46] Hofmann Ph, Gayone J E, Bihlmayer G, Koroteev Yu M and Chulkov E V 2005 Electronic structure and fermi surface of Bi(100) *Phys. Rev.* B **71** 195413

[47] Hirahara T *et al* 2007 Direct observation of spin splitting in bismuth surface states *Phys. Rev.* B **76** 153305

[48] Nicolay G, Reinert F, Hüfner S and Blaha P 2001 Spin–orbit splitting of the L-gap surface state on Au(111) and Ag(111) *Phys. Rev.* B **65** 033407

[49] Sugawara K, Sato T, Souma S, Takahashi T, Arai M and Sasaki T 2006 Fermi surface and anisotropic spin–orbit coupling of Sb(111) studied by angle-resolved photoemission spectroscopy *Phys. Rev. Lett.* **96** 046411

[50] Hsieh D *et al* 2009 Observation of unconventional quantum spin textures in topological insulators *Science* **323** 919–22

[51] Mönig H, Sun J, Koroteev Yu M, Bihlmayer G, Wells J, Chulkov E V, Pohl K and Hofmann Ph 2005 Structure of the (111) surface of bismuth: LEED analysis and first-principles calculations *Phys. Rev.* B **72** 085410

[52] Bihlmayer G, Koroteev Yu M, Echenique P M, Chulkov E V and Blgel S 2006 The Rashba-effect at metallic surfaces *Proc. 23th European Conf. on Surface Science (Berlin, Sept. 2005)*; *Surf. Sci.* **600** 3888–91

[53] Hirahara T *et al* 2008 Origin of the surface-state band-splitting in ultrathin Bi films: from a Rashba effect to a parity effect *New J. Phys.* **10** 083038

[54] Meier F, Dil J H and Osterwalder J 2009 Measuring spin polarization vectors in angle-resolved photoemission spectroscopy *New J. Phys.* submitted

[55] Hupalo M, Schmalian J and Tringides M C 2003 Devils staircase in Pb/Si(111) ordered phases *Phys. Rev. Lett.* **90** 216106

[56] Bihlmayer G, Blügel S and Chulkov E V 2007 Enhanced Rashba spin–orbit splitting in Bi/Ag(111) and Pb/Ag(111) surface alloys from first principles *Phys. Rev.* B **75** 195414

[57] Takayanagi K, Kolb D M, Kambe K and Lehmpfuhl G 1980 Deposition of monolayer and bulk lead on Ag(111) studied in vacuum and in an electrochemical cell *Surf. Sci.* **100** 407–22

[58] Rolland A, Bernardini J and Barthes-Labrousse M G 1984 Vapour deposition of lead on Ag(111) and equilibrium surface segregation from Ag–Pb(111) solid solutions: a LEED-AES comparative study *Surf. Sci.* **143** 579–90

[59] Dalmas J, Oughaddou H, Léandri C, Gay J-M, Le Lay G, Tréglia G, Aufray B, Bunk O and Johnson R L 2005 Ordered surface alloy formation of immiscible metals: the case of Pb deposited on Ag(111) *Phys. Rev.* B **72** 155424

[60] Pacilé D, Ast C R, Papagno M, Da Silva C, Moreschini L, Falub M, Seitsonen A P and Grioni M 2006 Electronic structure of an ordered Pb/Ag(111) surface alloy: theory and experiment *Phys. Rev.* B **73** 245429

[61] Ast C R, Henk J, Ernst A, Moreschini L, Falub M C, Pacilé D, Bruno P, Kern K and Grioni M 2007 Giant spin splitting through surface alloying *Phys. Rev. Lett.* **98** 186807

[62] Premper J, Trautmann M, Henk J and Bruno P 2007 Spin–orbit splitting in an anisotropic two-dimensional electron gas *Phys. Rev.* B **76** 073310

[63] Ast C R *et al* 2008 Spin–orbit split two-dimensional electron gas with tunable Rashba and Fermi energy *Phys. Rev.* B **77** 081407

[64] Meier F, Petrov V, Guerrero S, Mudry C, Patthey L, Osterwalder J and Dil J H 2009 Unconventional Fermi surface spin textures in the Bi_xPb_{1-x}/Ag(111) surface alloy *Phys. Rev.* B **79** 241408

[65] Ast C R, Wittich G, Wahl P, Vogelgesang R, Pacilé D, Falub M C, Moreschini L, Papagno M, Grioni M and Kern K 2007 Local detection of spin–orbit splitting by scanning tunneling spectroscopy *Phys. Rev.* B **75** 201401

[66] Cappelluti E, Grimaldi C and Marsiglio F 2007 Electron–phonon effects on spin–orbit split bands of two-dimensional systems *Phys. Rev.* B **76** 085334

[67] Cappelluti E, Grimaldi C and Marsiglio F 2007 Topological change of the Fermi surface in low-density Rashba gases: application to superconductivity *Phys. Rev. Lett.* **98** 167002

[68] Srisongmuang B, Pairor P and Berciu M 2008 Tunneling conductance of a two-dimensional electron gas with Rashba spin–orbit coupling *Phys. Rev.* B **78** 155317

[69] Mirhosseini H, Henk J, Ernst A, Ostanin S, Chiang C-T, Yu P, Winkelmann A and Kirschner J 2009 Unconventional spin topology in surface alloys with Rashba-type spin splitting *Phys. Rev.* B **79** 245428

[70] de Vries S A, Huisman W J, Goedtkindt P, Zwanenburg M J, Bennett S L, Robinson I K and Vlieg E 1998 Surface atomic structure of the reconstructions of Ag(111) and Cu(111) *Surf. Sci.* **414** 159–69

[71] Soares E A, Bittencourt C, Nascimento V B, de Carvalho V E, de Castilho C M C, McConville C F, de Carvalho A V and Woodruff D P 2000 Structure determination of Ag(111)(3×3)R30°–Sb by low-energy electron diffraction *Phys. Rev.* B **61** 13983–7

[72] Moreschini L *et al* 2009 Assessing the atomic contribution to the Rashba spin–orbit splitting in surface alloys: Sb/Ag(111) *Phys. Rev.* B **79** 075424

[73] Mans A, Dil J H, Ettema A R H F and Weitering H H 2002 Quantum electronic stability and spectroscopy of ultrathin Pb films on Si(111)7×7 *Phys. Rev.* B **66** 195410

[74] Hirahara T, Nagao T, Matsuda I, Bihlmayer G, Chulkov E V, Koroteev Yu M, Echenique P M, Saito M and Hasegawa S 2006 Role of spin–orbit coupling and hybridization effects in the electronic structure of ultrathin Bi films *Phys. Rev. Lett.* **97** 146803

[75] Dil J H, Kampen T U, Hülsen B, Seyller T and Horn K 2007 Quantum size effects in quasi-free-standing Pb layers *Phys. Rev.* B **75** 161401

[76] Castro Neto A H, Guinea F, Peres N M R, Novoselov K S and Geim A K 2009 The electronic properties of graphene *Rev. Mod. Phys.* **81** 109

[77] Chiang T C 2000 Photoemission studies of quantum well states in thin films *Surf. Sci. Rep.* **39** 181–235

[78] Zhang Z, Niu Q and Shih C-K 1998 Electronic growth of metallic overlayers on semiconductor substrates *Phys. Rev. Lett.* **80** 5381–4

[79] Budde K, Abram E, Yeh V and Tringides M C 2000 Uniform, self-organized, seven-step height Pb/Si(111) $-$ (7×7) islands at low temperatures *Phys. Rev.* B **61** R10602–5

[80] Kirchmann P S, Wolf M, Dil J H, Horn K and Bovensiepen U 2007 Quantum size effects in Pb/Si(111) investigated by laser-induced photoemission *Phys. Rev.* B **76** 075406

[81] Aballe L, Barinov A, Locatelli A, Heun S and Kiskinova M 2004 Tuning surface reactivity via electron quantum confinement *Phys. Rev. Lett.* **93** 196103

[82] Jałochowski M, Hoffman M and Bauer E 1996 Quantized hall effect in ultrathin metallic films *Phys. Rev. Lett.* **76** 4227–9

[83] Orr B G, Jaeger H M and Goldman A M 1984 Transition-temperature oscillations in thin superconducting films *Phys. Rev. Lett.* **53** 2046–9

[84] Koitzsch C, Battaglia C, Clerc F, Despont L, Garnier M G and Aebi P 2005 Photoemission of a quantum cavity with a nonmagnetic spin separator *Phys. Rev. Lett.* **95** 126401

[85] Schiller F, Keyling R, Chulkov E V and Ortega J E 2005 Surface state scattering at a buried interface *Phys. Rev. Lett.* **95** 126402

[86] Shikin A M and Rader O 2007 Valence-band splitting in Mg/W(110): neither spin–orbit nor parity effect *Phys. Rev.* B **76** 073407

[87] Shikin A M, Varykhalov A, Prudnikova G V, Usachov D, Adamchuk V K, Yamada Y, Riley J D and Rader O 2008 Origin of spin–orbit splitting for monolayers of Au and Ag on W(110) and Mo(110) *Phys. Rev. Lett.* **100** 057601

[88] Varykhalov A, Sánchez-Barriga J, Shikin A M, Gudat W, Eberhardt W and Rader O 2008 Quantum cavity for spin due to spin–orbit interaction at a metal boundary *Phys. Rev. Lett.* **101** 256601

[89] He K, Hirahara T, Okuda T, Hasegawa S, Kakizaki A and Matsuda I 2008 Spin polarization of quantum well states in Ag films induced by the Rashba effect at the surface *Phys. Rev. Lett.* **101** 107604

[90] Frantzeskakis E, Pons S, Mirhosseini H, Henk J, Ast C R and Grioni Marco 2008 Tunable spin gaps in a quantum-confined geometry *Phys. Rev. Lett.* **101** 196805

[91] Matsuda I, Ohta T and Yeom H W 2002 In-plane dispersion of the quantum-well states of the epitaxial silver films on silicon *Phys. Rev.* B **65** 085327
[92] Aballe L, Rogero C, Kratzer P, Gokhale S and Horn K 2001 Probing interface electronic structure with overlayer quantum-well resonances: Al/Si(111) *Phys. Rev. Lett.* **87** 156801
[93] Milun M, Pervan P and Woodruff D P 2002 Quantum well structures in thin metal films: simple model physics in reality? *Rep. Prog. Phys.* **65** 99–141
[94] Dil J H, Kim J W, Gokhale S, Tallarida M and Horn K 2004 Self-organization of Pb thin films on Cu(111) induced by quantum size effects *Phys. Rev.* B **70** 045405
[95] Upton M H, Wei C M, Chou M Y, Miller T and Chiang T-C 2004 Thermal stability and electronic structure of atomically uniform Pb films on Si(111) *Phys. Rev. Lett.* **93** 026802
[96] Hirahara T, Nagao T, Matsuda I, Bihlmayer G, Chulkov E V, Koroteev Yu M and Hasegawa S 2007 Quantum well states in ultrathin Bi films: angle-resolved photoemission spectroscopy and first-principles calculations study *Phys. Rev.* B **75** 035422
[97] Upton M H, Miller T and Chiang T-C 2005 Unusual band dispersion in Pb films on Si(111) *Phys. Rev.* B **71** 033403
[98] Dil J H, Kim J W, Kampen Th, Horn K and Ettema A R H F 2006 Electron localization in metallic quantum wells: Pb versus In on Si(111) *Phys. Rev.* B **73** 161308
[99] Altfeder I B, Chen D M and Matveev K A 1998 Imaging buried interfacial lattices with quantized electrons *Phys. Rev. Lett.* **80** 4895–8
[100] Ricci D A, Miller T and Chiang T-C 2004 Chemical tuning of metal–semiconductor interfaces *Phys. Rev. Lett.* **93** 136801
[101] Ricci D A, Liu Y, Miller T and Chiang T-C 2009 Analyticity of the phase shift and reflectivity of electrons at a metal–semiconductor interface *Phys. Rev.* B **79** 195433
[102] Geim A K and Novoselov K S 2007 The rise of graphene *Nat. Mater.* **6** 183–191
[103] Kane C L and Mele E J 2005 Quantum spin Hall effect in graphene *Phys. Rev. Lett.* **95** 226801
[104] Huertas-Hernando D, Guinea F and Brataas A 2006 Spin–orbit coupling in curved graphene, fullerenes, nanotubes, and nanotube caps *Phys. Rev.* B **74** 155426
[105] Dedkov Yu S, Fonin M, Rudiger U and Laubschat C 2008 Rashba effect in the graphene/Ni(111) system *Phys. Rev. Lett.* **100** 107602
[106] Rader O, Varykhalov A, Sánchez-Barriga J, Marchenko D, Rybkin A and Shikin A M 2009 Is there a Rashba effect in graphene on 3d ferromagnets? *Phys. Rev. Lett.* **102** 057602
[107] Varykhalov A, Sánchez-Barriga J, Shikin A M, Biswas C, Vescovo E, Rybkin A, Marchenko D and Rader O 2008 Electronic and magnetic properties of quasifreestanding graphene on Ni *Phys. Rev. Lett.* **101** 157601
[108] Ohta T, Bostwick A, Seyller T, Horn K and Rotenberg E 2006 Controlling the electronic structure of bilayer graphene *Science* **313** 951–4
[109] Fu L, Kane C L and Mele E J 2007 Topological insulators in three dimensions *Phys. Rev. Lett.* **98** 106803
[110] Fu L and Kane C L 2007 Topological insulators with inversion symmetry *Phys. Rev.* B **76** 045302
[111] Kane C L and Mele E J 2005 Z2 topological order and the quantum spin Hall effect *Phys. Rev. Lett.* **95** 146802
[112] Xia Y *et al* 2009 Observation of a large-gap topological-insulator class with a single Dirac cone on the surface *Nat. Phys.* **5** 398
[113] Zhang H, Liu C-X, Qi X-L, Dai X, Fang Z and Zhang S-C 2009 Topological insulators in Bi_2Se_3, Bi_2Te_3 and Sb_2Te_3 with a single Dirac cone on the surface *Nat. Phys.* **5** 438
[114] Hsieh D *et al* 2009 A tuneable topological insulator in the spin helical Dirac transport regime *Nature* **460** 1101
[115] Fu Liang and Kane C L 2009 Probing neutral majorana fermion edge modes with charge transport *Phys. Rev. Lett.* **102** 216403
[116] Akhmerov A R, Nilsson J and Beenakker C W J 2009 Electrically detected interferometry of majorana fermions in a topological insulator *Phys. Rev. Lett.* **102** 216404
[117] Crain J N, Kirakosian A, Altmann K N, Bromberger C, Erwin S C, McChesney J L, Lin J-L and Himpsel F J 2003 Fractional band filling in an atomic chain structure *Phys. Rev. Lett.* **90** 176805
[118] Tegenkamp C, Kallassy Z, Pfnür H, Günter H-L, Zielasek V and Henzler M 2005 Switching between one and two dimensions: conductivity of Pb-induced chain structures on Si(557) *Phys. Rev. Lett.* **95** 176804
[119] Tegenkamp C, Ohta T, McChesney J L, Dil H, Rotenberg E, Pfnür H and Horn K 2008 Coupled Pb chains on Si(557): origin of one-dimensional conductance *Phys. Rev. Lett.* **100** 076802
[120] Wells J W *et al* 2009 Nondegenerate metallic states on Bi(114): a one-dimensional topological metal *Phys. Rev. Lett.* **102** 096802
[121] Krupin O, Bihlmayer G, Starke K, Gorovikov S, Prieto J E, Dobrich K, Blugel S and Kaindl G 2005 Rashba effect at magnetic metal surfaces *Phys. Rev.* B **71** 201403